Received: 8 November 2024 | Revised: 20 March 2025 | Accepted: 12 May 2025

DOI: 10.1002/qj.5032

Quarterly Journal of the Royal Meteorological Society RMetS

RESEARCH ARTICLE

How sensitive are Sahelian mesoscale convective systems to cold-pool suppression?

Ben Maybee[1] | **James Bassford**[1] | **John H. Marsham**[1] | **Huw Lewis**[2] | **Paul Field**[2] | **Cornelia Klein**[3] | **Douglas J. Parker**[1,4,5]

[1]School of Earth and Environment, University of Leeds, Leeds, UK

[2]Met Office, Exeter, UK

[3]UK Centre for Ecology and Hydrology (UKCEH), Wallingford, UK

[4]National Centre for Atmospheric Science (NCAS), University of Leeds, Leeds, UK

[5]NORCE Norwegian Research Centre AS, Bjerknes Center for Climate Research, Bergen, Norway

Correspondence
Ben Maybee, School of Earth and Environment, University of Leeds, Leeds, UK.
Email: b.w.maybee@leeds.ac.uk

Funding information
Natural Environment Research Council, Grant/Award Numbers: NE/W001888/1, NE/X017419/1

Abstract

Understanding the physical processes driving deep convective storms is an essential prerequisite for understanding the wider tropical atmosphere. Cold pools driven by rainfall evaporation are a ubiquitous feature of mesoscale convective systems (MCSs) that have especially pronounced upscale effects in the climate of the West African Sahel, through their modulation of the regional monsoon circulation. The role of cold pools in determining the dynamics, life cycle, and propagation of tropical MCSs themselves, however, remains debated. Here, we probe the feedback of cold pools on Sahelian MCS characteristics through a 40-day, 2.2 km convection-permitting Met Office Unified Model sensitivity experiment in which rainfall evaporation is switched off in the microphysics scheme. Storms generated in the sensitivity experiment subsequently show strongly suppressed cold-pool density currents versus a control simulation. Yet we find no statistically significant difference between the diurnal cycles of MCS counts, with continued nocturnal propagation of storms in the experiment, and a reduction of MCS speeds by 1.7 $m \cdot s^{-1}$ caused by a similar slowdown in the African easterly jet due to a weakened large-scale meridional temperature gradient. Indeed, the main differences between the simulations are in the regional mean state and diurnal cycles of MCS rainfall. Changes to composite updraught geometry are consistent with the role of cold-pool horizontal vorticity in balancing the strong low-level wind shear characteristic of the region. Remarkably though, we find no sensitivity of the positive scaling of MCS rainfall with shear to cold pools, with reduced entrainment dilution under stronger shear conditions the fundamental physics driving the relationship. Our results help to disentangle processes in the Sahel in which cold pools play a driving role (nocturnal rainfall intensification, regional circulation) from those in which they are passive actors, which we find primarily to be MCS development, propagation, and rainfall–shear scalings.

KEYWORDS

cold pools, convection-permitting modelling, MCSs, West African Sahel, wind shear

1 | INTRODUCTION

It is frequently stated that convective cold pools play an essential role in the dynamics of mesoscale convective systems (MCSs). MCSs are an archetypal form of convective organisation, comprising clusters of thunderstorms that merge to form large, cold anvil clouds. Their structure is complex and comprised of features spanning a wide range of scales from high, cold anvil shields spanning thousands of square kilometres, to sub-kilometre entrainment and microphysical processes (Houze, 2004). Evaporation of rainfall from multiple embedded kilometre-scale convective updraughts leads to cooling of ambient air and the formation of downdraughts; this cool, negatively buoyant air sinks, forming convective cold pools at the MCS base. These form multiple propagating density currents that can merge to form large, organised systems with rich structures (Drager & van den Heever, 2017; Fuglestvedt & Haerter, 2020).

Cold pools are one of MCSs' most striking observed features, typically causing significant decreases in surface temperature, increases in surface pressure, strong winds, and an increase in relative humidity as the ambient surface layer is displaced by their cool, dense air (Engerer *et al.*, 2008; Provod *et al.*, 2016). They are features common to all flavours of convective rainfall, and an integral component of convective organisation across scales (Bony *et al.*, 2015; Tompkins, 2001). Gust fronts at cold-pool boundaries enable the triggering of new convective cells through both moisture convergence and mechanical lifting (Torri *et al.*, 2015), with cold-pool collisions enhancing this effect (Fuglestvedt & Haerter, 2020; Meyer & Haerter, 2020). Idealised large-eddy simulations, typically using experiments where rainfall evaporation is turned off and cold pools inhibited, show that cold pools play a critical role in the transition from shallow to deep convection (Khairoutdinov & Randall, 2006), but that their impact on organisation is a nonlinear function of domain size (Jeevanjee & Romps, 2013).

In mature MCSs, cold pools are canonically understood to maintain mature storms and determine their updraught geometry (Rotunno–Klemp–Weisman [RKW] theory; Rotunno *et al.*, 1988) by providing a balance to the horizontal vorticity generated by low-level vertical wind shear. Predictions derived from such arguments for the speeds, shear–relative orientation, and updraught tilts of midlatitude MCSs are well verified by idealised numerical experiments (Abramian *et al.*, 2022; Bryan *et al.*, 2006; Robe & Emanuel, 2001; Weisman & Rotunno, 2004). However, experiments again turning off rainfall evaporation in both idealised and realistic model set-ups have shown repeatedly that MCSs can continue to initiate, mature, and propagate without cold pools (Clark *et al.*, 2014; Crook & Moncrieff, 1988; Grant *et al.*, 2018, 2020; Schumacher, 2009; Stoelinga *et al.*, 2003; Trier *et al.*, 2011). Moreover, MCS rainfall in observed storms increases under stronger environmental shear (Chen *et al.*, 2023; Hsiao *et al.*, 2024; Senior *et al.*, 2021). This positive feedback can be explained without reference to cold pools, through shear modulation of low-level unstable inflow (Alfaro, 2017; Bickle *et al.*, 2021) causing a decrease in updraught entrainment rates at higher shear found in both idealised experiments (Abramian *et al.*, 2023; Mulholland *et al.*, 2021) and regional simulations with explicit convection (Maybee *et al.*, 2024).

Questions surrounding the role of cold pools in MCS dynamics are of great practical importance in the semi-arid Sahel region of West Africa, some parts of which receive over 90% of their seasonal rainfall totals from the long-lived propagating MCSs (Mathon *et al.*, 2002) supported by strong wind shear between the low-level monsoon flow and midlevel African easterly jet (AEJ; Parker & Diop-Kane, 2017). These MCSs form huge, country-scale cold pools (Hoeller *et al.*, 2024; Provod *et al.*, 2016), generating cool, moist outflows into the Sahara that mediate the northerly propagation of the West African monsoon (Birch *et al.*, 2014a; Marsham *et al.*, 2013; Trzeciak *et al.*, 2017). Convective cold-pool misrepresentation in models leads to significant biases both in Saharan temperatures and dust transport (Garcia-Carreras *et al.*, 2013, 2021; Marsham *et al.*, 2011). Wind shear exercises important controls on MCSs in this region, with stronger shear due to a strengthening meridional temperature gradient responsible for an observed intensification in extreme MCS rainfall (Taylor *et al.*, 2017). Global climate models underpinning projections of future Sahel rainfall do not resolve this mechanism, with projections of extremes significantly increased when combined with observed MCS rainfall–shear scalings (Klein *et al.*, 2021). Though thermodynamic drivers naturally provide the leading control on projected trends in the regions' MCSs (Bickle *et al.*, 2021; Zhao *et al.*, 2024), the physics of MCS–shear interactions, and thus cold pools, is a crucial component of improving climate projections in the Sahel.

A common adjective in the preceding paragraphs is "idealised": many results underpinning our understanding of MCS dynamics ultimately stem from high-resolution large-eddy simulations under idealised scenarios. Yet MCSs are well simulated by kilometre-grid-scale convection-permitting (CP) models, despite such models' parametrisation of many smaller scale processes (Crook *et al.*, 2019; Prein *et al.*, 2017), with results for many key characteristics very similar to large-eddy-simulation-scale models (Prein *et al.*, 2021). Multiple state-of-the-art global CP models can now be run on climate time-scales while resolving MCSs (Donahue *et al.*, 2024; Hohenegger

et al., 2023; Rackow *et al.*, 2024), explicitly embedding the dynamics and forcings of MCSs into global simulations (Feng *et al.*, 2023; Slingo *et al.*, 2022). Such advances in computing capabilities provide an opportunity to test questions regarding the dynamics of MCSs under far more realistic experimental configurations, including all environmental interactions, and on much larger MCS sample sizes. In this context, some CP models can now capture the observed positive feedback of shear on MCS rainfall, provided they simulate a decrease in entrainment-dilution with shear (Maybee *et al.*, 2024), with errors in simulated rainfall–shear response explaining spatial biases in West African MCS mean rainfall and diabatic heating.

The results of Maybee *et al.* (2024) highlight the importance of evaluating how MCSs interact with wind shear. The role of convective cold pools, and the surrounding debate regarding their role in MCS dynamics, was not considered. Here, we focus on this question for the Sahel by comparing MCSs between two 40-day CP simulations, described in Section 2, that differ only by switching off rainfall evaporation in one experiment. In Section 3 we show that convective cold pools are thus suppressed in our experiment; despite this, however, long-lived, mature MCSs that propagate deep into the night still form. We consider the changes to interactions with wind shear in Section 4, finding limited change in the leading-order scalings of key MCS fields (rainfall, brightness temperature) when cold pools are suppressed. We discuss how our results intersect the existing literature in Section 5, especially regarding MCS maintenance, before concluding in Section 6.

2 | DATA AND METHODS

Here, we detail the two simulations ("Control" and "RainEvapOff"), MCS tracking methods (simpleTrack; Stein *et al.*, 2014), and key diagnostic measures used in our study. Both Control and RainEvapOff are 2.2 km grid regional CP simulations conducted using the non-hydrostatic, semi-Lagrangian Met Office Unified Model (MetUM; Brown *et al.*, 2012).

2.1 | Experimental set-up

The common modelling set-up we utilise is the limited-area model configuration first described by Jones *et al.* (2023)—also LAM2.2 in Maybee *et al.* (2024). The two experiments span a large North African domain (−13°–28°N, −20°–54°E) for 40 days from August 1, 2016, to September 9, 2016. Both feature a 2.2 km horizontal grid spacing and 90 vertical levels up to 40 km. Lateral boundary conditions are derived from an N1280 (∼ 10 km spacing at the Equator) global simulation initialised from a MetUM operational analysis, with additional forcing from daily updating sea-surface temperatures. Deep convection is explicitly represented through adoption of the convection-permitting RAL3.2 science configuration (Bush *et al.*, 2023, 2024), which includes an explicitly represented land surface (Best *et al.*, 2011), a bimodal large-scale cloud parametrisation scheme (Van Weverberg *et al.*, 2021), and CASIM, a double-moment microphysics scheme (Field *et al.*, 2023). For simplicity, the impact of aerosols is ignored and the in-cloud droplet number concentration is fixed at $\sim 150\ \mathrm{cm}^{-3}$, but the rain droplet number can evolve freely.

The only difference between Control and RainEvapOff stems from the CASIM microphysics scheme. In RainEvapOff, evaporation of rainfall was switched off at all levels.[1] Other species' evaporation parameters (e.g., ice, graupel) remain active, and no modifications were made in the cloud scheme. No modifications are made to CASIM in Control. An alternative compiler optimisation setting was also used for RainEvapOff, but this will not make any difference to the model diagnostics. In both simulations, two-dimensional fields were outputted on hourly time steps, and (instantaneous) three-dimensional fields onto pressure levels at three-hourly intervals.

2.2 | MCS tracking

To identify MCSs and study their full life cycle, from initiation to dissipation, we use the simpleTrack algorithm of Stein *et al.* (2014), which has been used extensively to track MCSs from both observational and model data (Crook *et al.*, 2019; Feng *et al.*, 2025; Tomassini *et al.*, 2023). The algorithm uses a single two-dimensional field and tracks clusters that meet prescribed cut-off and area thresholds. We refer to individual clusters that form part of an MCS track as snapshots. To join temporally disparate clusters into storm tracks, a velocity field is calculated from cross-correlation of two contiguous time steps. By using this field, snapshots in the earlier time step are advected forwards to the later time. Snapshots where the fractional overlap in the later time step between the advected and "true" cluster is greater than 0.6 are then considered part of the same storm track. A new initiation is considered to have occurred if no overlap is found with an advected cluster, whereas multiple advected clusters overlapping a single cluster in the later time step are considered a merge of those storm tracks (Stein *et al.*, 2014).

Here, we track MCSs from top-of-atmosphere brightness temperature (BT), calculated from total outgoing long-wave radiation using the empirical conversion of Yang and Slingo (2001). We track storms over West Africa

(here −6°–24°N, −18°–32°E) only, where the monsoon, and thus MCS activity, is at its peak during the simulation period. The tracking algorithm is applied to 0.1° regridded fields (equivalent to observational products), with a minimum cluster area of nine pixels ($\lesssim$ 1,000 km^2) and BT threshold of 241 K (−32°C), as adopted in a recent intercomparison of MCS tracking algorithms (Feng *et al.*, 2025). Upon completion, candidate MCSs are selected as tracks where, during the storm life cycle, a maximum area > 5,000 km^2 and minimum BT < 223 K (−50°C) are achieved. For these tracks, snapshot rainfall volumes and extremes are calculated from precipitation on the same 0.1° grid. MCSs are then further required to reach a maximum rainfall rate above 1 mm · hr^{-1} during the storm's lifetime. Finally, we restrict our attention to MCSs in the Sahel by excluding track initiations outside 9°–19°N and −10°–24°E.

We are particularly interested in the convective dynamics of mature MCSs, which we identify after tracking as contiguous subregions of BT below −50°C with area larger than 5,000 km^2 within a tracked snapshot. MCS mergers can cause individual tracked snapshots to be formed from multiple mature storm regions, where individual cores' convective dynamics are well isolated and distinct. Field composites for mature MCSs are thus centred on the location of the minimum BT (BT_{min}) of all distinct, unconnected mature subregions of a track snapshot. We restrict our sample of mature MCSs to those east of −12°E to avoid sampling oceanic storms.

2.3 | Process evaluation

To distinguish cold-pool characteristics between Control and RainEvapOff we use buoyancy b (Tompkins, 2001), which we calculate from the virtual potential temperature θ_v:

$$b = \frac{g(\theta_v - \overline{\theta}_v)}{\overline{\theta}_v}, \quad (1)$$

where g is Earth's gravitational field and $\overline{\theta}_v$ is the mean value across a 100×100 km^2 bounding box (Prein *et al.*, 2021). Note that buoyancy should be calculated from density potential temperature θ_ρ, which further includes mixing ratios for cloud condensate and rain water in addition to water vapour; these microphysical diagnostics were unfortunately not available for the long simulations used here. We therefore use θ_v as the closest possible approximation. Cold-pool outflow boundaries can then be approximately located by identifying regions with strong gradients in θ_v (Drager and van den Heever (2017)).

To evaluate the role of cold pools in MCS environmental interactions, we consider only mature MCS regions during the hours of peak convection (1600–2100 UTC) that themselves have a maximum rainfall rate > 1 mm · hr^{-1}. We define the environmental conditions for such storms as the preceding 1200 UTC mean field across a 0.7° box centred on the location of the mature MCS BT_{min} (Klein *et al.*, 2021). As in Maybee *et al.* (2024), we represent MCSs' thermodynamic and dynamical environments by total column integrated water vapour (TCW) and the difference between 850 hPa and 650 hPa zonal winds ($u_{850} - u_{650}$) respectively, where the latter measure is henceforth referred to as shear. The choice of shear measure corresponds physically to the difference between the AEJ and southwesterly monsoon flow, and roughly spans heights between 1 and 3.5 km above the surface.

We follow Baidu *et al.* (2022) and Maybee *et al.* (2024) and evaluate changes in entrainment-dilution with shear by calculating two proxies for bulk entrainment:

$$w_{eff} = \frac{w500_{max}}{\sqrt{CAPE_{env}}} \quad \text{and} \quad BT_{diff} = T_{anv} - LNB_{env}, \quad (2)$$

where $w500_{max}$ is the maximum 500 hPa vertical velocity within the mature MCS footprint, $CAPE_{env}$ is the convective available potential energy of the storm's mean environmental sounding, T_{anv} is the mean mature MCS anvil temperature (i.e., mean BT, < −50°C), and LNB_{env} is the level of neutral buoyancy of the mean environmental sounding. Together, these variables provide a consistent picture of how bulk entrainment-dilution varies: entrainment reduces the potential of a near-surface parcel to reach its theoretical maximum buoyancy. Since this reduces w and increases T_{anv} (i.e, lowers anvil heights), reduced entrainment-dilution will correspond to high w_{eff}, the efficiency of conversion of CAPE, and low BT_{diff}, the difference between anvil and LNB heights (Baidu *et al.*, 2022; Maybee *et al.*, 2024). Mulholland *et al.* (2021) showed that growth in convective core areas with shear yields the noted decrease in entrainment. We measure convective cores using the area of the strongest contiguous subregion where w_{500} is greater than the 99th percentile of its in-storm values (i.e., under the mature MCS footprint). Our threshold criteria for mature MCSs ensures this measure is the same as in Maybee *et al.* (2024).

3 | MCS LIFE CYCLES

Here, we examine the structure of cold pools of 1800 UTC MCSs in Control and RainEvapOff, before turning to the effect of suppressing rainfall evaporation on the diurnal cycle and nocturnal propagation of MCSs. To contextualise our MCS-level results however, we begin by looking at

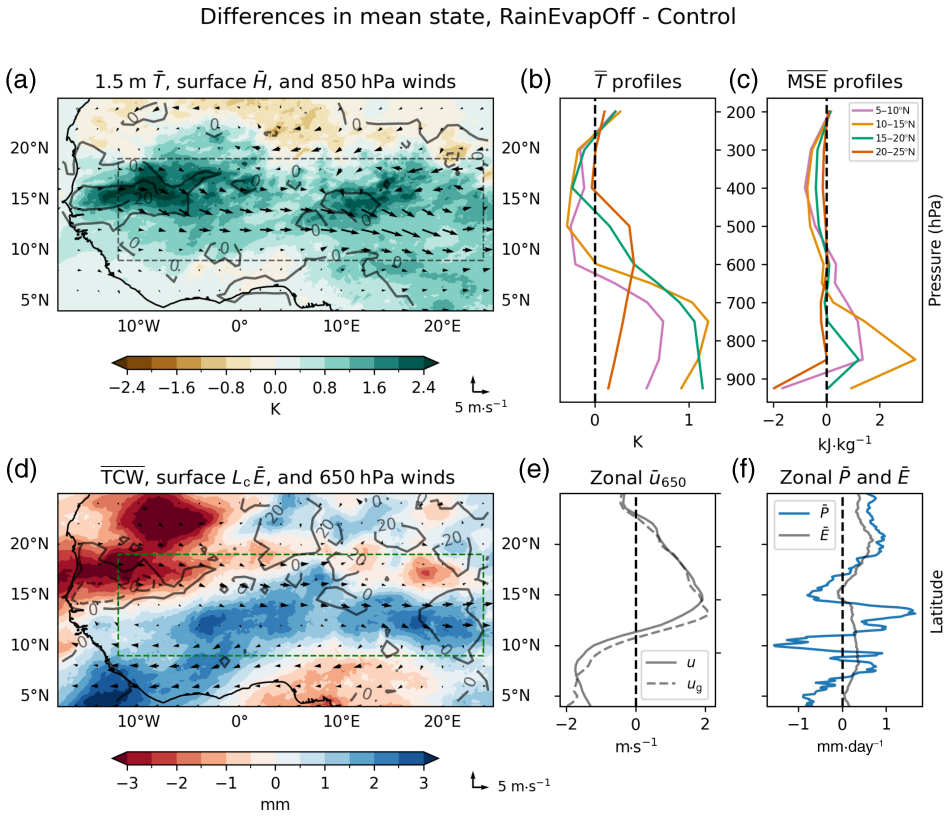

FIGURE 1 Differences between mean fields in RainEvapOff and Control. (a) Difference in 1.5 m mean air temperature $\overline{T}$ and 850 hPa wind fields (every 2° by 2°). Vertical profiles of differences in (b) $\overline{T}$ and (c) mean moist static energy $\overline{MSE}$ shown for four distinct latitude bands. (d) Difference in mean total column integrated water vapour (TCW; shading), mean surface latent heat flux $L_c\bar{E}$ (20 W · m^{-2} grey contours), and 650 hPa wind fields (every 2° by 2°), accompanied in (e) by difference in zonal mean total and geostrophic zonal flow, u and u_g. (f) Difference in zonal mean daily precipitation and evaporation totals. Dashed boxes in (a) and (d) denote Sahel study region. [Colour figure can be viewed at wileyonlinelibrary.com]

the effect of removing rainfall evaporation on the mean atmospheric state.

3.1 | Background mean state

As expected, turning off rainfall evaporation removes the associated sub-cloud cooling. Large parts of the domain are warmer near the surface in RainEvapOff (Figure 1a), with much of the domain south of 20°N having 0.5–2 K higher mean 1.5 m air temperatures. The mean depth of the temperature difference reaches at least 650 hPa at all latitudes in the domain (Figure 1b). The deepest and largest low-level temperature differences are concentrated in the Sahel (dashed box), especially in the west. RainEvapOff shows increased westerly flow across the Sahel at 850 hPa (Figure 1a), corresponding to a strengthening of the climatological winds at this level.

What of differences in atmospheric moisture? Vertical profiles of mean moist static energy (MSE) in Figure 1c show a similar increase in RainEvapOff at low levels in all regions except the Sahara, with the strongest differences versus Control again in the Sahel. Above 600 hPa, however, all regions show reduced MSE in RainEvapOff. Integrating through the column, the spatial distribution of TCW (Figure 1d) shows higher values in RainEvapOff across most of the Sahel and south to the Gulf of Guinea coastline. However, there is a strong drying in the western Sahara (and weaker drying over orography). As implied by the MSE profiles, the increased TCW in RainEvapOff is primarily due to increased boundary-layer moisture, with a slight dry bias at midlevels (Supporting Information Figure S1a). This translates into raised CAPE values in RainEvapOff—for example, the distribution of environmental CAPE values preceding mature MCSs (Supporting Information Figure S2) shows a significant positive shift.

RainEvapOff has higher low-level temperatures and more rainfall reaching the surface, leading to additional latent heat fluxes (contours) into a warmer lower atmosphere that can hold more vapour. A consequence of this is raised low-level humidity across the Sahel and parts of the Sahara. In contrast, mean sensible heat flux (contours, Figure 1a) is generally higher in Control, whereas moisture convergence associated with the monsoon flow is similar in both simulations (Supporting Information Figure S1b), pointing to the importance of surface evaporation. Mean diurnal cycles for the Sahel show consistent partitioning of the surface fluxes in the two simulations (Supporting Information Figure S3), with increased Bowen ratio in RainEvapOff, but no changes to the timings of changes in low-level moisture or boundary-layer depth. In addition to the role of surface evaporation and monsoon flow in enhancing low-level humidity in RainEvapOff, there may also be significant effects from the likely suppression of convective downdraughts and cold pools, which play a key thermodynamic role through injecting ambient air into

the boundary layer (Provod *et al.*, 2016; Tompkins, 2001). The differences in TCW and 850 hPa winds are consistent with the drying and deepening of the Saharan heat low (Supporting Information Figure S1c), increasing localised low-level cyclonic flow. This is consistent with a further synoptic-scale signature of cold-pool suppression, since cold pools play key roles in ventilating the Saharan heat low with cool, moist air from the south (Garcia-Carreras *et al.*, 2013; Marsham *et al.*, 2013; Trzeciak *et al.*, 2017).

Comparing winds at the AEJ level of 650 hPa, we find that, similar to 850 hPa, winds are generally more westerly in RainEvapOff (Figure 1d). Here, however, this represents a slowing of the mean easterly flow. The zonal mean of the difference in 650 hPa zonal wind (Figure 1e) shows an inflection at $\sim 12°$N, with reduced easterly flow in RainEvapOff versus Control across most of the Sahel. This change is consistent with the alteration to thermal wind balance resulting from the distribution of temperature increases in RainEvapOff, as shown by close alignment with the zonal mean differences in the geostrophic component u_g. Over West Africa, geopotential height is approximately a function solely of temperature; consequently, thermal wind can be described, to close approximation, by the vertically varying geostrophic flow. The changes in the zonal wind differences in Figure 1e align with a strengthened meridional temperature gradient over 4°–12°N in Figure 1a, and weakened gradient from 12°–20°N, the latter of which weakens the easterly flow.

Finally, Figure 1f shows the difference in zonal mean daily precipitation totals $\overline{P}$. The design of our sensitivity experiment suppresses the loss of rainfall mass to water vapour—yet, interestingly, rainfall in RainEvapOff is not higher everywhere in the monsoon region, with higher rainfall rates in Control at the coast, 10°N, and 16°N. Only at 16°N can this be explained by relatively higher zonal mean evaporation $\bar{E}$ in Control. In RainEvapOff, the coastal rainfall is shifted northwards, but the biggest increases are in the core Sahel band and Sahara. The latter increase is likely since the majority of rainfall would typically evaporate in the lower atmosphere under the very high temperatures and low relative humidities. The increase in the Sahel, where MCSs dominate the climatology, points to the expected increased efficiency of storm rainfall when evaporation is suppressed.

In summary, switching off rainfall evaporation causes significant changes to the West African monsoon. Across the Sahel, the boundary layer is warmer, moister, and more convectively unstable in RainEvapOff, with increased latent heat fluxes compensating for decreased atmospheric evaporation. The weakened Sahara–Sahel meridional temperature gradient enhances the westerly component of the low-level monsoon flow but weakens the midlevel easterly flow across the region. Total precipitation is increased over the Sahel but decreases over other regions of West Africa.

3.2 | Cold-pool structure

As a qualitative illustration of the fundamental differences in MCS structure between RainEvapOff and Control, Figure 2 shows the footprint of a westward-propagating MCS at 1800 UTC on August 1, 2016. We use the time of peak convection on the first day for this comparison to ensure that divergence between the two experiments is still small. In the Control MCS (Figure 2a), strong regions of negatively buoyant air at 925 hPa are collocated with two intense convective updraughts demarcated by high rainfall rates. The collocation of these regions behind the linear $|\nabla\theta_v|$ contour (yellow), orthogonal to the direction of propagation, denotes the existence of a large, organised convective cold-pool density current propagating ahead of the MCS convection but located within the footprint of the anvil shield (BT = −32°C contour, dashed). Ahead of the cold pool's leading edge, the air is very buoyant, suggesting low-level storm inflow being mechanically lifted by the cold pool.

In Figure 2b, we see that, despite the MCS generating higher rainfall rates without evaporation, there is no formation of a significant cold pool. There are some small, disconnected negatively buoyant regions around the convective core, with several dispersed $|\nabla\theta_v|$ contour features nearby; these features will be generated by the evaporation of graupel and ice species. This evaporation is enough to generate some small surface cold pools, but not the large, organised density current seen in Control. There is also no clear low-level inflow region of positively buoyant air.

Figure 2c plots the difference in 925 hPa $|\nabla\theta_v|$ between RainEvapOff and Control across the entire region, giving a wider view of the cold-pool characteristics at this time. The region is dominated by numerous arc-shaped (open to the east) tight peaks of Control (purple) $|\nabla\theta_v|$, showing the strong changes in buoyancy associated with very large convective cold pools. In contrast, no such features are seen for RainEvapOff (orange), which are instead limited to tightly bound dense clusters of contours as seen in Figure 2b. However, this does not indicate an absence of MCSs; markers showing the locations of mature MCS locations from both simulations show a roughly comparable number of features between Control and RainEvapOff. There are MCSs in RainEvapOff at this early time step, and they do not have canonical cold pools. Note that the dominant MCS propagation direction is westwards (i.e., easterly) across the Sahel, with less than 10% of storms in either simulations propagating east (Supporting Information Figure S4a).

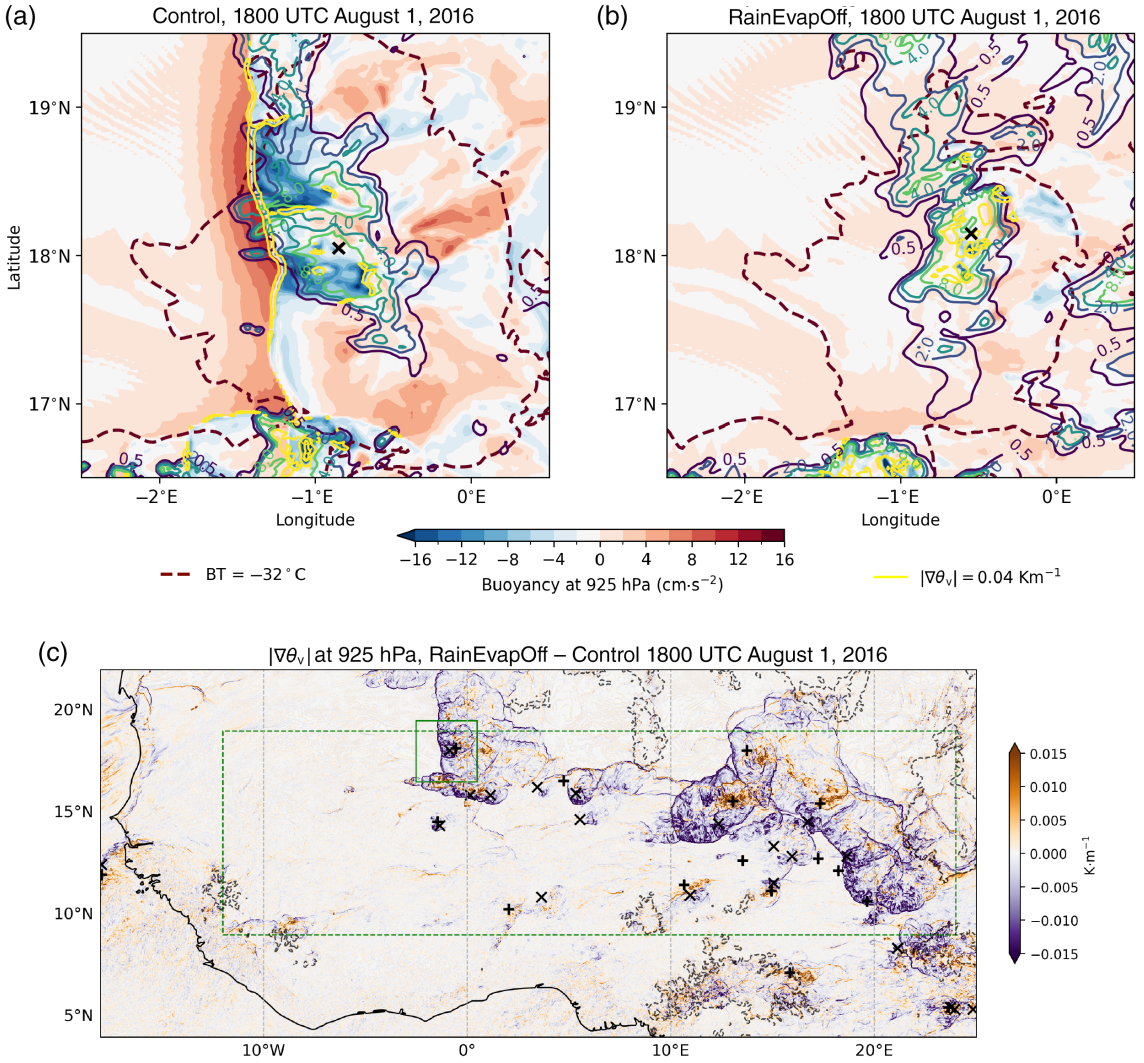

FIGURE 2 Representative mesoscale convective system (MCS) structures at the same location in (a) Control and (b) RainEvapOff at 1800 UTC on August 1, 2016. Colour shading shows buoyancy at 925 hPa (cm · s^{-2}); labelled solid blue–green contours show mean hourly rainfall rates (mm · hr^{-1}). Dashed bold contour shows MCS anvil footprint (BT < −32°C), and unlabelled yellow contours show boundaries where $|\nabla\theta_v| = 0.04$ K · m^{-1} at 925 hPa. (c) Difference in $|\nabla\theta_v|$ field at 925 hPa across West Africa between RainEvapOff and Control at 1800 UTC on August 1, 2016. Location of tracked mature MCS BT_{min} locations at this time in RainEvapOff (Control) shown by + (×) markers. Solid box indicates region in panels (a) and (b); dashed box denotes Sahel study region. Dashed contours shown for surface elevations of 750 m and 1,500 m. [Colour figure can be viewed at wileyonlinelibrary.com]

These illustrative results are taken for one time step, soon after simulation initialisation. Figure 3 shows the differences in mean composite cold-pool structure at 1800 UTC between Control and RainEvapOff for the full 40 days. Both simulations show comparable numbers of mature MCSs, with composites taken around 462 BT_{min} locations in RainEvapOff and 415 in Control.

As anticipated, cold pools are on average stronger and larger in Control. Figure 3a displays an ∼ 100 km westward arc focused on the composite centre where the negative buoyancy in Control is > 0.8 cm · s^{-2} stronger. Buoyancy is more negative for MCSs in Control everywhere 100 km behind (i.e., trailing) this arc, and is more positive than RainEvapOff west of $x = -50$. The strongest difference in wind anomalies is collocated with the arc, with stronger easterly winds in Control indicative of gust fronts at cold pools' leading edges. In RainEvapOff, evaporation of graupel and ice is clearly able to generate localised negatively buoyant regions, with dense air at the composite centre and behind the mean core location (Figure 3b). However, this "mean cold pool" is much weaker and more limited in extent than its counterpart for MCSs in Control (cf. Figure 3c).

The qualitative differences in cold-pool structures seen in Figure 2 are borne out in the composites. In Control there is a negative zonal gradient of equivalent potential

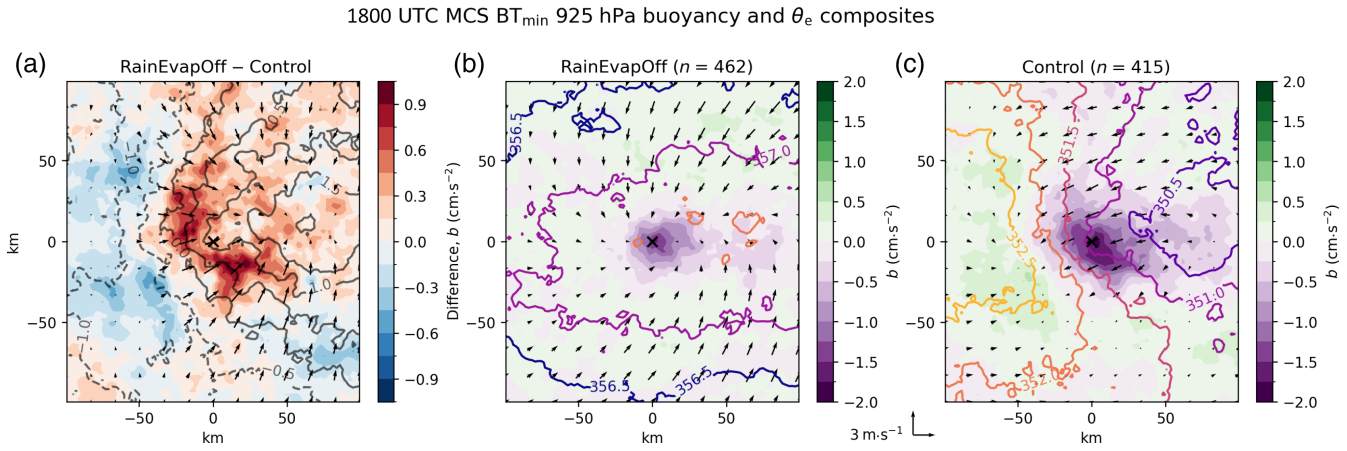

FIGURE 3 (a) Difference between (b) RainEvapOff and (c) Control 1800 UTC mature mesoscale convective system composite mean 925 hPa buoyancy (cm · s^{-1}, shading), equivalent potential temperature θ_e (0.5 K contours), and spatial anomalies of storm-relative winds (m · s^{-1}, common barb scale). Storm speeds taken from instant velocity values outputted by simpleTrack algorithm, with wind field coarsened for display purposes. Values *n* indicate composite sample sizes; composite centre "core" location marked by black cross. [Colour figure can be viewed at wileyonlinelibrary.com]

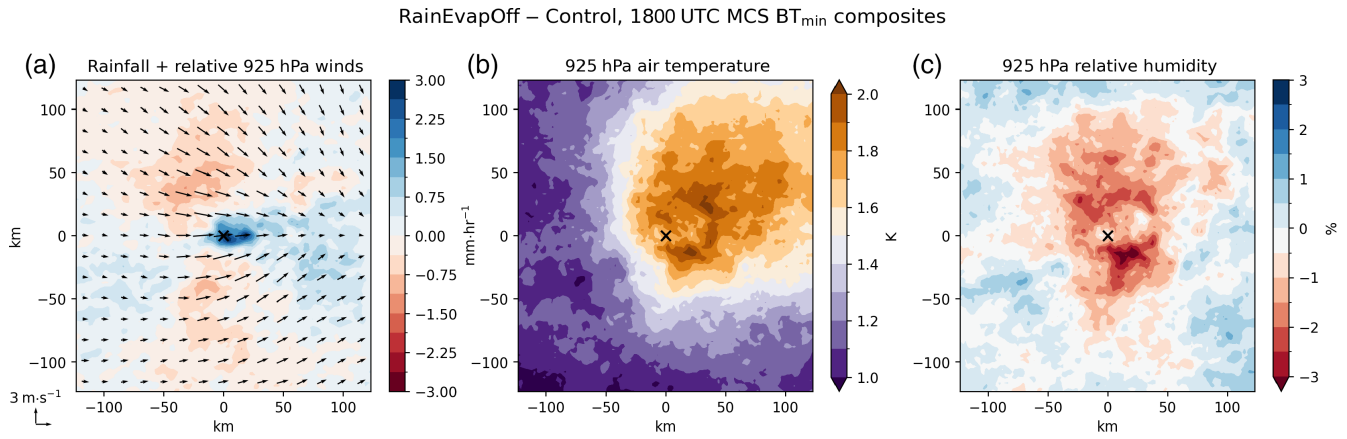

FIGURE 4 Differences in 1800 UTC mature mesoscale convective system composite mean (a) rainfall (mm · hr^{-1}) and 925 hPa storm-relative winds, (b) 925 hPa air temperature (K), and (c) relative humidity (%) between RainEvapOff and Control. Storm-relative winds obtained as in Figure 3. [Colour figure can be viewed at wileyonlinelibrary.com]

temperature across the MCS, and easterly wind anomalies east of $x = -50$ only. Since low-level inflow to storms' convective cores is typically moist and convectively unstable (high CAPE), inflow is anticipated from high-θ_e regions. The fields in Figure 3c are thus consistent with a squall line with (westerly) low-level inflow from positively buoyant air ascending over a (easterly) cold-pool gust front ahead of the deep convection, and moreover agree with observations of monsoon-season MCSs (Provod *et al.*, 2016). Meanwhile, in RainEvapOff, the θ_e gradient is positive, with peak values behind the composite centre, where a "sink" in the predominantly meridional wind anomalies lies. This points to the evolution of a very different MCS structure in the absence of rainfall evaporation, a point we investigate further in Section 4.

Figure 4a further shows the differences in composite MCS rainfall and absolute 925 hPa storm-relative winds between the experiments. Close to the BT_{min} core location rainfall is significantly higher in RainEvapOff than in Control, as expected from our experimental design. Rates are also higher in RainEvapOff in the region of weaker stratiform rainfall east of (i.e., following) the composite centre. However, directly north and south of the centre the rainfall is more than 1 mm · hr^{-1} higher in Control. A similar pattern is repeated in composites for brightness temperatures, with lower values in Control on this axis (Supporting Information Figure S5). These results are caused by the systematic difference in MCS structure between the two experiments: large cold pools in Control form westward-propagating linear squall lines (exemplified by

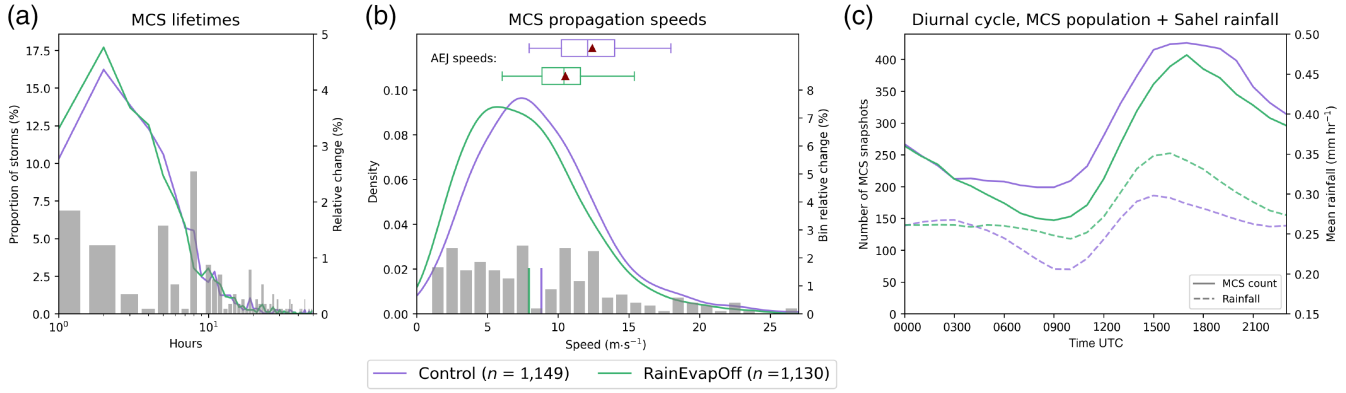

FIGURE 5 Life-cycle statistics for Sahel mesoscale convective system (MCS) tracks in Control (purple) and RainEvapOff (green). (a) MCS lifetimes binned on 1 hr intervals. Grey bars show percentage change of bin counts in RainEvapOff relative to Control. (b) Continuous probability density functions (PDFs, lines) and relative 1 $m \cdot s^{-1}$ bin differences (grey bars) for MCS propagation speeds; continuous PDF derived using a Gaussian kernel density estimate with a maximum value of 30 $m \cdot s^{-1}$. Vertical lines on *x*-axis denote distribution means. Horizontal box plots show distribution of daily mean zonal African easterly jet (AEJ) speeds, with distribution means indicated by triangles. (c) Hourly total counts of tracked MCS snapshots (solid lines) and mean Sahel rainfall (dashed). Values *n* in legend specify number of independent MCS tracks. [Colour figure can be viewed at wileyonlinelibrary.com]

Figure 2) with further convective cells on the meridional axis neighbouring the composite-centred core, in contrast to the dominant isolated features about which composites are taken in RainEvapOff. This is further evidenced in Figure 4a by the collocation of the strongest zonal wind differences, corresponding to strengthened easterly flow in Control from the cold-pool density currents, with regions where rainfall is higher in Control.

The mean effect of MCS propagation on 925 hPa temperature and moisture is shown in Figure 4b,c. Whereas air is warmer everywhere in RainEvapOff (Figure 1), this is notably enhanced over an area larger than 100 km^2 close to and behind the core mean location, indicating the pronounced effect of the cold pools in Control on air temperatures under and behind MCSs. The central 100 km^2 region is meanwhile more humid in Control (Figure 4c), despite the higher ambient humidity in RainEvapOff shown around the composite edges. On average, MCS convection in RainEvapOff is associated with far weaker decreases in temperature, and increases in humidity, of low-level ambient air than Control. Both signals are indicators of the passage of observed Sahelian cold pools (Hoeller *et al.*, 2024), further showing a strong suppression of cold pools in RainEvapOff.

3.3 | Diurnal cycle

The results of the previous section confirm the expectation that removing rainfall evaporation strongly suppresses convective cold pools, at least at the diurnal peak of convection. Maybe more intriguing is the persistent ability of mature MCSs to form without these cold pools. This could be explained by short-lived convection, generated by the significant ambient convective instability in the afternoon Sahel boundary layer, which struggles to maintain the organised structures overnight. Figure 5 shows that this is emphatically not the case: the lifetimes of both experiments' MCS populations (Figure 5a) peak at 2 hr. A weak positive effect of cold pools on longevity is suggested by 3% more storms living for 3 hr or less in RainEvapOff, versus 4% more storms living between 5 and 9 hr in Control. However, in both simulations, ~15% of MCSs are long-lived storms that persist for 10 hr or more.

Figure 5b shows that MCS propagation speeds are on average lower in RainEvapOff, with a population peak 1.7 $m \cdot s^{-1}$ lower (23%) than in Control and mean speed 0.9 $m \cdot s^{-1}$ (10%) lower—a two-sided Student's *t* test verifies that the change in the means is significant ($P < 0.01$). Here, the MCS propagation speed is calculated as the geodesic distance between the initial and final track snapshot locations, divided by the number of hours between them (Crook *et al.*, 2019). The suppression of cold pools in RainEvapOff may yield a direct, dynamical reduction in MCS speed; however, MCS propagation speed in the Sahel is primarily determined by the steering flow of the AEJ (Bickle *et al.*, 2021). Approximating the AEJ strength in the experiments as the daily maximum zonal-mean easterly wind determined from a 2° rolling meridional mean from 10°N to 20°N, we find a significant decrease in the distribution of daily AEJ strength in RainEvapOff of 1.9 $m \cdot s^{-1}$ ($P < 0.01$ under *t* test). This is comparable to the decrease in MCS propagation speeds. The weakening of the background 650 hPa easterly winds, and thus AEJ, in RainEvapOff is due to changes in thermal wind balance resulting from increased low-level temperatures that

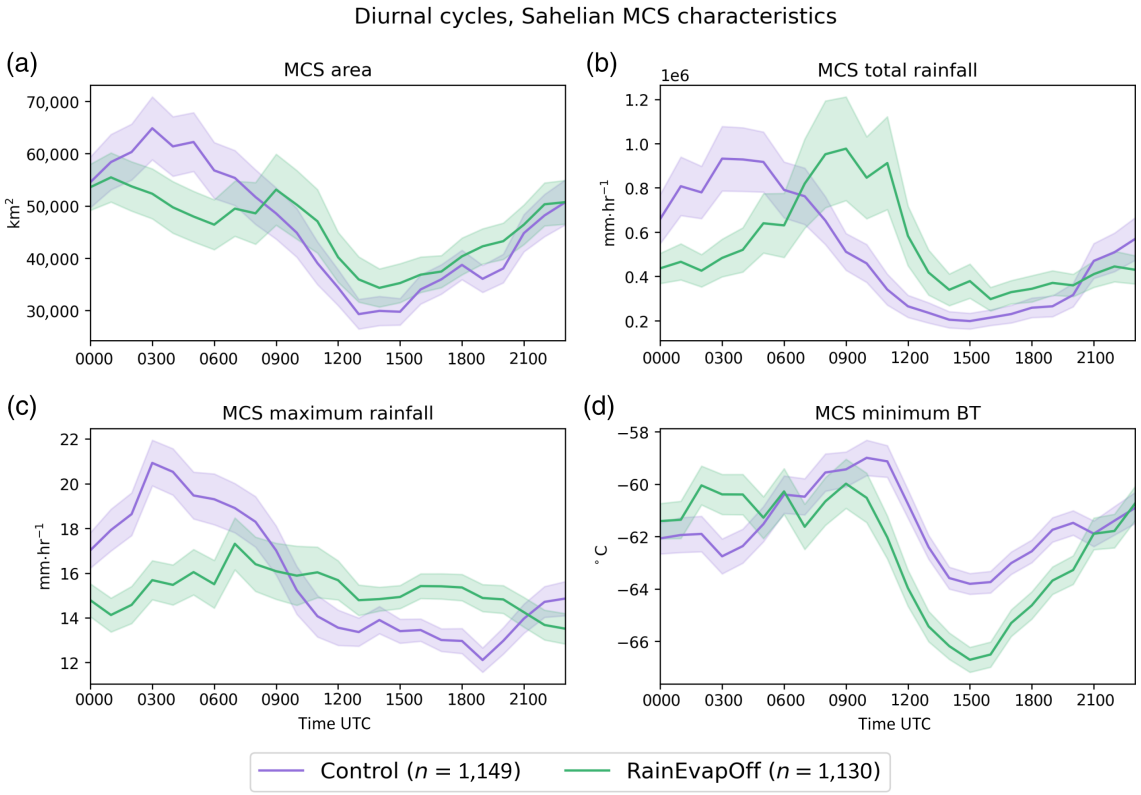

FIGURE 6 Mean diurnal cycles of tracked Sahelian mesoscale convective system (MCS) (a) snapshot anvil areas (km^2), (b) total rainfall (sum of rainfall rates within MCS area; $mm \cdot hr^{-1}$), (c) maximum rainfall ($mm \cdot hr^{-1}$), and (d) minimum brightness temperature BT (°C) in Control (purple) and RainEvapOff (green). Shading denotes standard error on the mean. Hourly means taken excluding values above the hourly 95th percentile for areas and rainfall to exclude interference from outlier values. All values calculated from 0.1° regridded fields. [Colour figure can be viewed at wileyonlinelibrary.com]

weaken the meridional temperature gradient (Figure 1). The primary influence of cold pools on the MCS speeds is thus likely indirect, through their contribution to the mean thermodynamic state. Note that the MCS speeds are derived from the outgoing long-wave radiation field alone and may differ from that of the cold-pool density currents.

The continued nocturnal maintenance of MCSs in RainEvapOff is confirmed by the diurnal cycle of the MCS snapshots that piece together the storm tracks (Figure 5c, solid lines). The timing and gradients of the cycles are generally similar, reflecting similar initiation and dissipation rates (Supporting Information Figure S2); the two count distributions are equivalent under a two-sample Kolmogorov–Smirnov test ($P = 0.26$). Whereas the shape of the diurnal cycle of the MCS populations mirrors that of all rainfall over the Sahel (Figure 5c, dashed lines), total regional rainfall is higher in RainEvapOff except around 0000 UTC. However, fewer storms persist into the early hours of the morning in RainEvapOff. There is a divergence in storm counts after 0300 UTC, with RainEvapOff showing 26% fewer MCSs at the diurnal minimum of 0900 UTC. This is despite an increase in regional rainfall versus Control—individual MCSs fractionally contribute higher rainfall amounts in RainEvapOff at this time. Note that morning initiation rates are also higher in Control (Supporting Information Figure S2b), where cold-pool outflows provide local convergence lines that aid convective development, and the peak in regional rainfall is earlier in the day, consistent with the role of cold pools in allowing upscale organisation. These differences not withstanding, nowhere does the MCS count in either simulation get close to zero, with the RainEvapOff minimum still corresponding to persistence of more than four MCSs a day on average.

The different behaviour of early morning storms in RainEvapOff is reinforced by mean diurnal cycles plotted in Figure 6. In Control, a nocturnal (0300 UTC) peak in MCS area, total and maximum rainfall, and accompanying secondary minimum in BT point to intense MCSs at that time, consistent with observations (Vizy & Cook, 2018). This peak is missing for RainEvapOff, which shows a single, lower diurnal minimum in MCS BT driven by primary storm initiation and fuelled by higher environmental CAPE (Supporting Information Figure S2); relatively constant maximum rainfall rates, and the highest total rainfall amounts during the period of least convective activity. The

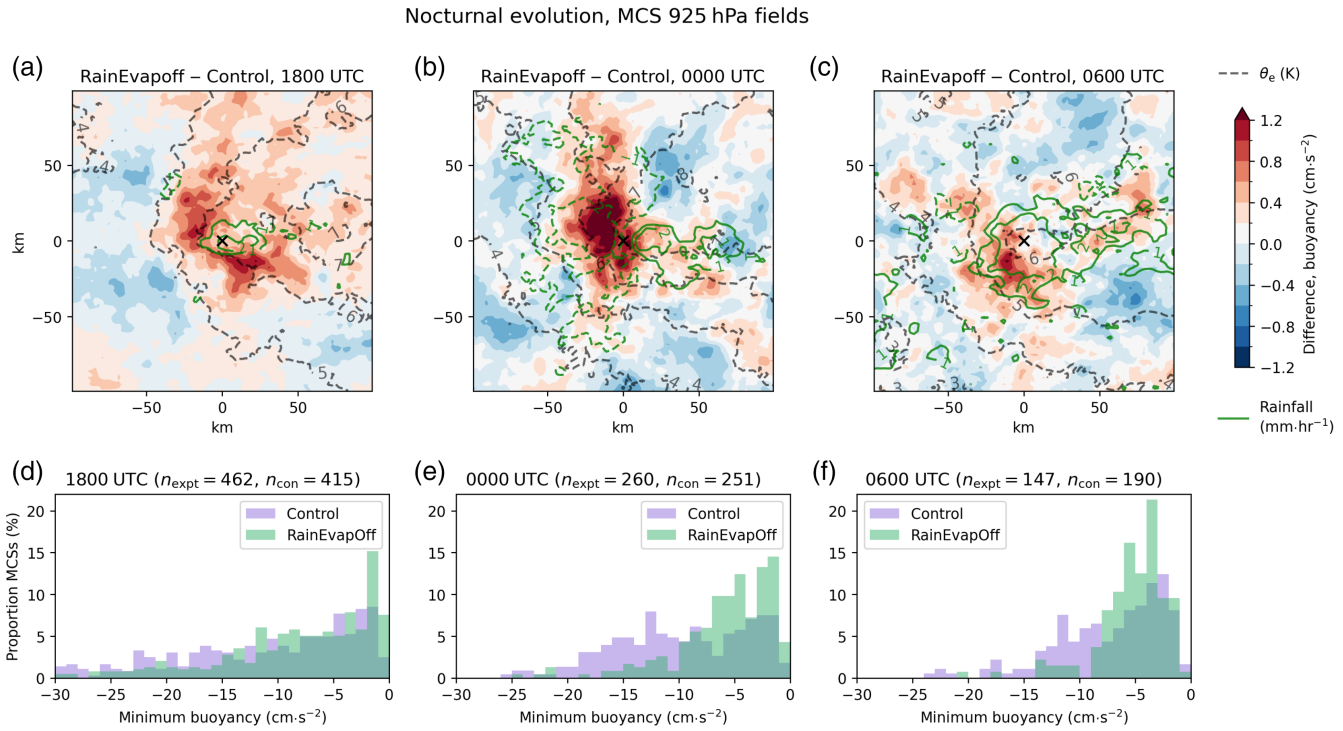

FIGURE 7 (a)–(c) Differences in mature mesoscale convective system (MCS) composite mean 925 hPa buoyancy (shading, $\mathrm{cm \cdot s^{-2}}$), 925 hPa equivalent potential temperature (dashed grey 1 K contours), and surface rainfall (green 1 $\mathrm{mm \cdot hr^{-1}}$ contours) between RainEvapOff and Control at 1800 UTC, 0000 UTC, and 0600 UTC. (d)–(e) Histograms of minimum 925 hPa buoyancy at the same times, sampled within 100 km box centred on mature MCS core locations. [Colour figure can be viewed at wileyonlinelibrary.com]

peak in mean storm area is 16% lower and 2 hr earlier than in Control. Together, these differences show that inhibiting rainfall evaporation suppresses mechanisms through which nocturnal MCSs can continue to intensify after the peak in convective activity. In RainEvapOff, only the strongest, largest storms continue to propagate beyond early morning, leading to the markedly later peak in total storm rainfall.

To understand the role of cold pools in the simulations' differing nocturnal MCS convection, Figure 7 shows the overnight evolution of the differences in cold-pool buoyancies between RainEvapOff and Control. The 1800 UTC mean composites (Figure 7a) again display enhanced differences in buoyancy west of the composite centre location, stronger differences in θ_e to the east, and enhanced RainEvapOff rainfall at the centre only. The distribution of MCS minimum buoyancy values (Figure 7d) is skewed towards more negative values in Control, indicating stronger buoyancies in Control stemming from large density currents beneath Control MCSs (e.g., Figure 3). This same qualitative pattern is maintained throughout the night in both spatial means and probability density functions; the nocturnal maintenance and propagation of MCSs in RainEvapOff is not explained by a small number of storms developing strong cold-pool features.

There are, however, some important nocturnal changes. At midnight, the difference in mean buoyancy is even stronger (Figure 7b): a strengthening of negative cold-pool buoyancy in Control is responsible, with a peak in minimum buoyancy developing at $-12\ \mathrm{cm \cdot s^{-2}}$ (Figure 7e) in Control only. A similar result holds for the distribution of mean buoyancy (Supporting Information Figure S6). This intensification explains the appearance of a dipole in rainfall differences, with a region of enhanced rainfall in the Control MCSs west of the centre (contours, Figure 7b). In all, the 0000 UTC MCSs in Control show strengthened cold pools simultaneous to early morning peaks in MCS rainfall and BT (Figure 6) that are absent in RainEvapOff. This indicates that the growth of large, organised convective cold pools is the mechanism driving the nocturnal peaks seen in Control. At 0600 UTC (Figure 7c,f) the cold-pool density currents in Control weaken relative to 0000 UTC but remain much stronger than counterparts in RainEvapOff.

4 | INTERACTIONS WITH WIND SHEAR

Cold pools are thought to play an important role in the interaction of mature MCSs with vertical wind shear

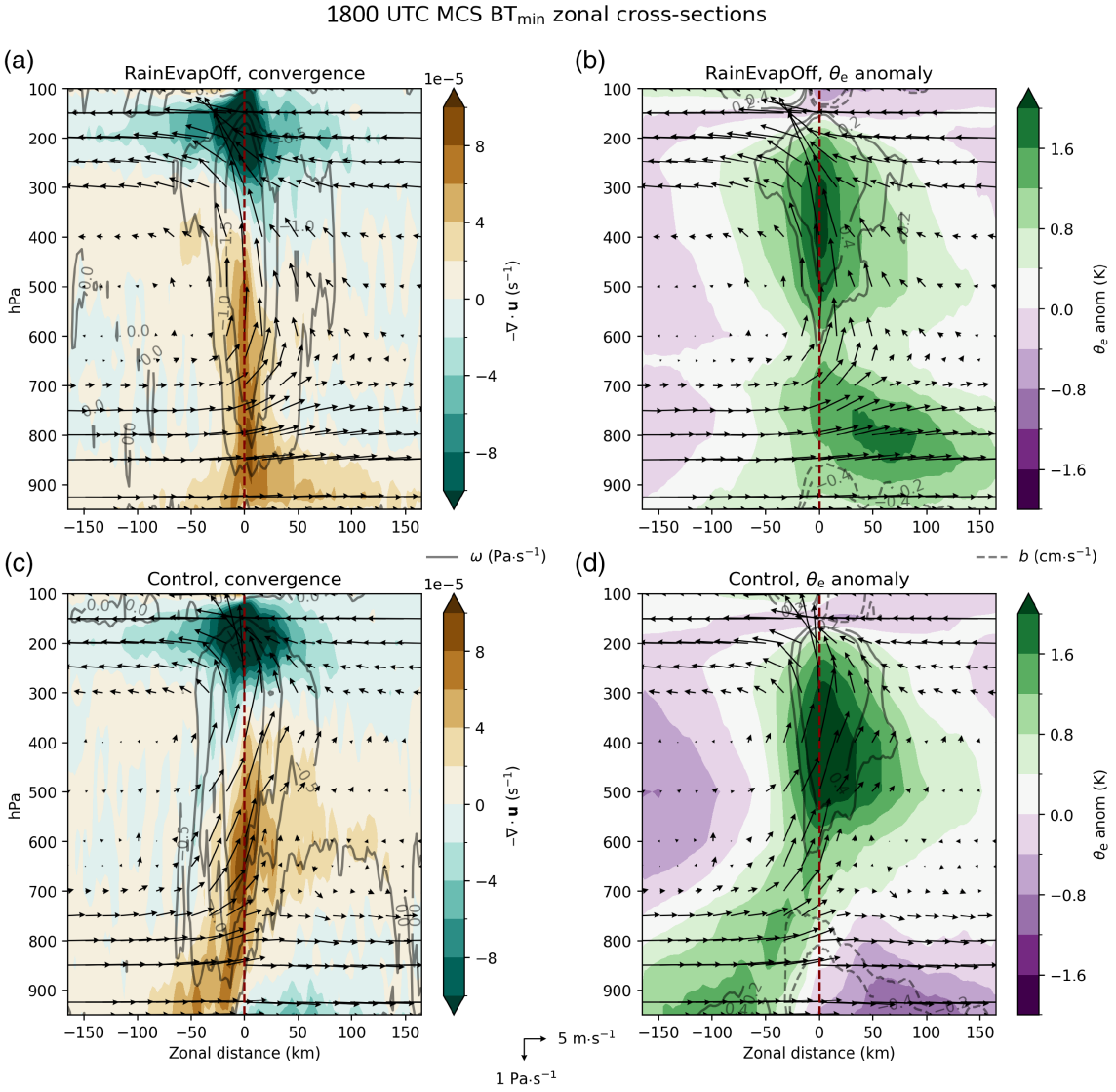

FIGURE 8 The 1800 UTC composite mean zonal sections over the central 50 km transect for mature mesoscale convective systems (MCSs) in (a–c) RainEvapOff and (b–d) Control. (a, c) Mean horizontal convergence (shading) and vertical velocity ω in pressure coordinates (0.2 Pa · s^{-1} contours); (b, d) mean equivalent potential temperature anomaly (shading) and buoyancy b (0.2 cm · s^{-1} contours), where θ_e anomaly is taken against the mean composite profile. Wind barbs show ω and storm-relative zonal wind components on common scale in plane of cross-section; storm-relative winds taken from instant velocity values outputted by the simpleTrack algorithm. Zonal wind field coarsened for display purposes. [Colour figure can be viewed at wileyonlinelibrary.com]

(Thorpe *et al.* (1982); Rotunno *et al.* (1988)). Here, we investigate the effect of suppressing cold pools on MCS updraught structure and shear controls on MCS rainfall.

4.1 | Updraught structure

We begin by comparing the zonal mean geometry of MCSs in Control and RainEvapOff. Figure 8 shows composite zonal mean vertical sections centred on 1800 UTC mature MCSs in both experiments; that is, along the $y = 0$ line for horizontal composites in Figures 3 and 4. The profile of horizontal convergence for MCSs in RainEvapOff (Figure 8a) shows a vertical region of strong convergence along the $x = 0$ axis. At low levels the strongest convergence is behind (east of) the centre line, extending up to 850 hPa for nearly 100 km; vertical velocities (contours) peak around 400 hPa at $x = 0$. The region of ascent is tilted slightly forwards, in the direction of propagation, with the convergence field suggesting low-level inflow primarily in the ∼75 km behind the composite centre.

This picture is confirmed by the mean zonal (composite anomaly) θ_e field, in which positive anomalies on a given level indicate relatively moist, warm air. Above 600 hPa, positive anomalies are focused around the $x = 0$ line, collocated with the strongest vertical velocities

in Figure 8a. Below 700 hPa, however, we see stronger positive anomalies behind the centre point (as in Figure 3b), further indicating this region is the source of low-level inflow air for the MCS's convective updraughts. Contours of buoyancy show that any localised negatively buoyant is weak and restricted to below 875 hPa.

MCSs in both experiments show divergent flow at 200 hPa above and ahead of the $x = 0$ line, indicating outflow from deep convective updraughts at the LNB. However, at mid and low levels, the vertical structure for MCSs in Control is very different. The region of strong convergence (Figure 8c) is primarily ahead of the composite centre near the surface, tilting backward for 100 km before straightening vertically above 650 hPa. Strong vertical ascent is found in this region and at all levels above, again peaking around 400 hPa. The 150 km east of the centre shows weak descending air, with $\omega > 0$ below 650 hPa and divergent flow below 800 hPa, indicating the presence of widespread convective downdraughts. Buoyancy contours in Figure 8d show the associated formation of deep convective cold pools at the surface, with a clear density current feature out to $x = -100$ km in the zonal mean.

The distribution of raised θ_e anomalies further points to backwards tilting updraughts, over the surface cold-pool density current, with low-level inflow sourced ahead of the MCS convection. The relative differences between the updraught and ambient air θ_e values are stronger in Control than in RainEvpOff, with generally higher buoyancies (both positive and negative), indicating stronger environmental contrasts and increased subsidence in Control, which shows midlevel divergence ahead of the convective region (Figure 8c). However, close to the composite core, updraught velocities are stronger at nearly all levels for MCSs in RainEvapOff (Supporting Information Figure S7a), with mean 500 hPa $\omega = -4.23$ Pa $\cdot$ s^{-1} in a 25 km square about the composite centre, versus -3.28 Pa $\cdot$ s^{-1} in Control. The stronger updraughts in RainEvapOff are a consequence of stronger low-level convergence than in Control (Supporting Information Figure S5b), and the significantly higher environmental CAPE values (Supporting Information Figure S2) due to the moister, warmer mean state.

The holistic differences in mean updraught structure between RainEvapOff and Control remain consistent through MCSs' nocturnal propagation, and we find far less pronounced differences in the meridional vertical composites, which are typically symmetric about the $y = 0$ axis (not shown). This is to be expected from the primarily westwards propagation of MCSs in both experiments, aligned with the strongest shear. Despite showing a weaker AEJ (Figure 5b), RainEvapOff shows very similar zonal shear values to Control due to the complimentary enhancement in low-level westerlies (Figure 1). The differences in the updraught structures, and tilt in particular, are thus consistent with RKW theory (Rotunno *et al.*, 1988), with the convective cold pools in Control providing negative meridional vorticity at low levels, and thus partly balancing the shear. In RainEvapoff there is no such balance and the tilt is forwards, although an absence of updraught weakening is in part due to the modified environmental conditions.

4.2 | MCS environmental response

Given the pronounced differences in mean updraught structure and shear interaction, the control of shear on the strength of MCS convection, measured through characteristics such as rainfall and BT, may be anticipated to also differ significantly between the experiments. Figure 9 shows this is not the case. The scalings of mature 1600–2100 UTC MCS maximum rainfall (Figure 9a), mean rainfall (Figure 9b), and minimum BT (Figure 9c) with 1200 UTC environmental shear strength are remarkably similar in the two experiments. For maximum rainfall the scaling is $\sim 20\%$ stronger in RainEvapOff; and whereas $\sim 10\%$ and $\sim 20\%$ weaker for RainEvapOff MCS mean rainfall and minimum BT respectively, there is no collapse in the shear response due to the absence of cold pools. Both experiments show similar dependence on TCW (Supporting Information Figure S8), but do have differing MCS number distributions (Supporting Information Figure S9), with stronger background shear in Control and a tighter clustering of MCSs near the mean AEJ speed in RainEvapOff.

We have previously shown that the increase of MCS rainfall with shear in Control—LAM2.2 in Maybee *et al.* (2024)—is explained by a decrease in bulk entrainment-dilution. Here, we find that this hypothesis remains true when rainfall evaporation is removed: Figure 9d,e consistently shows reduced bulk entrainment at high shear, with increased w_{eff} and decreased BT_{diff} values in these environments. The reduction of entrainment-dilution with shear explains the scalings of MCS rainfall and BT_{min} in both experiments, with significant correlations against the shear-binned entrainment measures. That this remains the case in RainEvapOff, where cold pools are strongly suppressed and there is no horizontal vorticity balance, indicates that entrainment-dilution effects are the leading-order mediator of shear controls on mature MCS convection.

There are important sub-leading effects apparent from the suppression of cold pools, however. The entrainment-dilution scalings are weaker in RainEvapOff, with consistently lower w_{eff} and higher BT_{diff} values

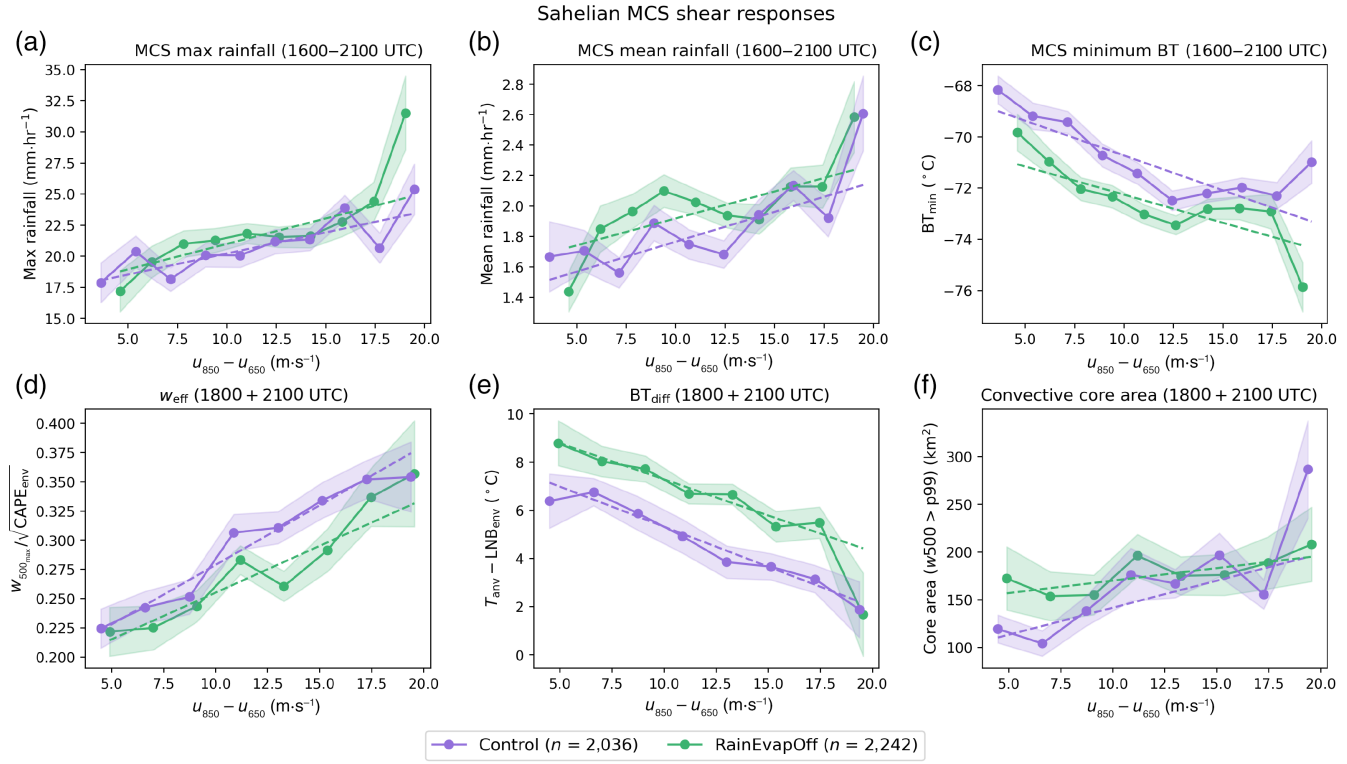

FIGURE 9 (a)–(c) The 1600–2100 UTC (a) maximum rainfall, (b) mean rainfall, and (c) minimum brightness temperature (BT) for mature mesoscale convective systems (MCSs) with maximum rainfall > 1 mm · hr^{-1}, binned by 1200 UTC environmental shear. Bins calculated between 5th and 95th shear percentile to remove extremes. (d)–(f) The 1800 + 2100 UTC MCS entrainment proxies (d) w_{eff} and (e) BT_{diff} and (f) 500 hPa core areas, similarly binned by shear. Difference in times due to three-hourly profile fields; values n indicate MCS sample sizes from 1600 to 2100 UTC. In all plots, shading denotes standard error on bin mean, and dashed lines indicate trend for error-weighted regression where gradient and correlation are significant at the 95% level. [Colour figure can be viewed at wileyonlinelibrary.com]

indicating higher bulk entrainment, likely a consequence of the drier midlevel mean state in RainEvapOff (Supporting Information Figure S1a). The positive feedback of cold pools is most apparent in the scaling of MCS convective core areas in Figure 9f, the growth of which with shear is understood to facilitate the reduction in entrainment rates (Mulholland *et al.*, 2021). Both experiments show a positive feedback of shear on core area size; however, the scaling in RainEvapOff is much weaker (half that in Control). This points to an important dynamical influence of MCS cold pools on updraught widths, and thus entrainment-dilution, leading to sub-leading effects on MCS rainfall. Cold-pool intensities typically increase with shear due to intensified rainfall evaporation (Abramian *et al.*, 2022), indicating a positive feedback of cold pools on MCS updraughts.

The intensification of MCS convection with environmental shear in both experiments agrees with previous results from observations (Hsiao *et al.*, 2024; Klein *et al.*, 2021); in contrast, an older MetUM climate simulation, CP4-Af, showed extremely weak shear controls on entrainment and rainfall (Maybee *et al.*, 2024; Senior *et al.*, 2021). Revisiting speculations in Maybee *et al.* (2024), our results here do not indicate that improvements in the MetUM microphysics parametrisation scheme, in particular the introduction of the two-moment CASIM scheme in the present RAL3 configuration, are responsible for this improvement in the MetUM. The primary influence of CASIM on the MCS shear response is expected to be through its essential role in generating cold pools, the suppression of which we have found does not weaken shear controls.

5 | DISCUSSION

In comparing MCSs between Control and RainEvapOff, two results stand out: there is no statistically significant difference between the diurnal cycles of MCS numbers in Control and RainEvapOff, with continued nocturnal maintenance and propagation of storms without rainfall evaporation (Figure 5); and suppressing cold pools makes little change to the dependence of MCS characteristics on shear (Figure 9), despite changes to storms' structures. The primary changes stemming from cold-pool suppression are instead to the diurnal cycle of rainfall and

the vertical structure of storms. These results are derived from large-domain CP simulations, which include realistic land-surface and radiation interactions.

To understand these results, first consider the maintained generation of Sahelian MCSs. The mechanical lifting provided by convective cold pools is often an essential component of convective initiation (Khairoutdinov & Randall, 2006; Torri *et al.*, 2015). In the Sahel, results from observations and CP simulations point to a key role of localised convergence (Dione *et al.* (2014); Birch *et al.* (2014a)), such as that generated along cold-pool gust fronts (Maurer *et al.*, 2017). However, local boundary-layer convergence can be generated independently; for example, through deep daytime rolls (Dione *et al.*, 2014), strong gradients in soil moisture (Taylor *et al.*, 2011), or by shifts in the Sahel intertropical discontinuity dryline (Vizy & Cook, 2018). The synoptic flow provides a further crucial control, with larger scale (300 km) convergence associated with 80% of initiations in a 40-day simulation (Birch *et al.*, 2014a). Thermodynamical changes to the mean state in RainEvapOff independently support MCS initiation. Enhanced latent heat fluxes into a warmer atmosphere raise boundary-layer moisture, yielding significantly enhanced CAPE values (Supporting Information Figure S2) for developing convective cells to access. Overall, the development of equivalent MCS numbers in RainEvapOff highlights the ability of mechanisms other than cold pools to contribute to triggering convection in the Sahel, with the increase in accessible CAPE in particular catalysing strong deep convective storm development.

Once mature, cold pools are not an essential component for developing an MCS. Pandya and Durran (1996) have shown that mature squall lines' mesoscale circulation can be generated by the strong thermal forcing provided by convective rainfall alone, solely through the nonlinear dynamics of gravity waves. The enhanced convective rainfall in RainEvapOff ensures such thermal forcing remains readily available, although the modified storm geometry may change the resultant circulation. Ultimately, though, the steady-state zonal circulation of a mature MCS is understood to depend fundamentally on a decrease in hydrostatic pressure around the updraught at midlevels; that is, a meso-low, preceded by a meso-high at upper levels over the trailing stratiform region (Houze, 2004; Moncrieff, 1992; Yang & Houze, 1996). Figure 10a,b shows that composite zonal sections of MCSs in both RainEvapOff and Control exhibit this structure, with negative geopotential anomalies at 500 hPa in the updraught region and positive anomalies near the tropopause behind the composite core. The generation of these pressure anomalies is independent of the storms' cold pools, whose primary effect is at the surface: in Control (Figure 10d) the cold pool causes a region of anomalously high pressure, with a fall of pressure in the later wake of the storm. In contrast, in RainEvapOff there is no surface high and low pressure precedes the MCS. This change does not affect the initiation of deep convection, due to the existence of other triggering mechanisms, and does not disrupt convective organisation generating the intrinsic mesoscale circulation of an MCS aloft.

Sustaining the steady-state MCS circulation in Figure 10 requires system propagation to maintain convectively unstable low-level inflow (Houze, 2004). Density current outflows provide only one of multiple such mechanisms. In the midlatitudes, squall lines can be maintained without cold pools where frontal dynamics or other mesoscale circulations provide low-level ascent (Schumacher, 2009; Stoelinga *et al.*, 2003; Trier *et al.*, 2011). Meanwhile, in the Tropics, coupling to external gravity waves can enable propagation (Crook & Moncrieff, 1988; Mapes *et al.*, 2003), especially for fast westward-moving tropical squall lines (Tulich & Kiladis, 2012). In low convective inhibition environments, convective interactions with internally generated gravity waves can control the maintenance and propagation of deep convection (Lane & Zhang, 2011; Liu & Moncrieff, 2004; Mapes, 1993; Tulich & Mapes, 2008). In particular, Grant *et al.* (2018) studied the relative role of cold pools and gravity wave interactions in maintaining mesoscale convection in idealised, weak-shear oceanic domains and found that suppressing cold pools caused no change to MCS propagation and speeds, indeed enhancing storm intensity, in a striking parallel to our results for the Sahel.

In contrast though, the Sahel is a strongly sheared tropical environment. Here, MCS initiation is controlled by large-scale, low-level convergence, which is observed to continue to influence the propagation of mature MCSs (Klein & Taylor, 2020). Large-scale convergence was shown to impact idealised MCSs by Crook and Moncrieff (1988), where, in experiments with no rainfall evaporation, convergence enabled the maintenance of convection despite the absence of cold pools. We find that this mechanism consistently explains our results showing the continued nocturnal propagation of Sahelian MCSs when rainfall evaporation is inhibited. Figure 11a shows that, at 0000 UTC, RainEvapOff indeed exhibits large-scale (300 km mean) convergence at 925 hPa across most of our Sahel study domain. In contrast, in Control, the wind field is generally divergent. The low-level flow in RainEvapOff is thus conducive to MCS maintenance through the mechanisms of Crook and Moncrieff (1988).

This difference between the Sahelian low-level flows in the two experiments is not a static feature, instead displaying a marked diurnal evolution. Figure 11b shows the strengthened zonal mean convergence in RainEvapOff is limited to between approximately 12°N and 18°N, and

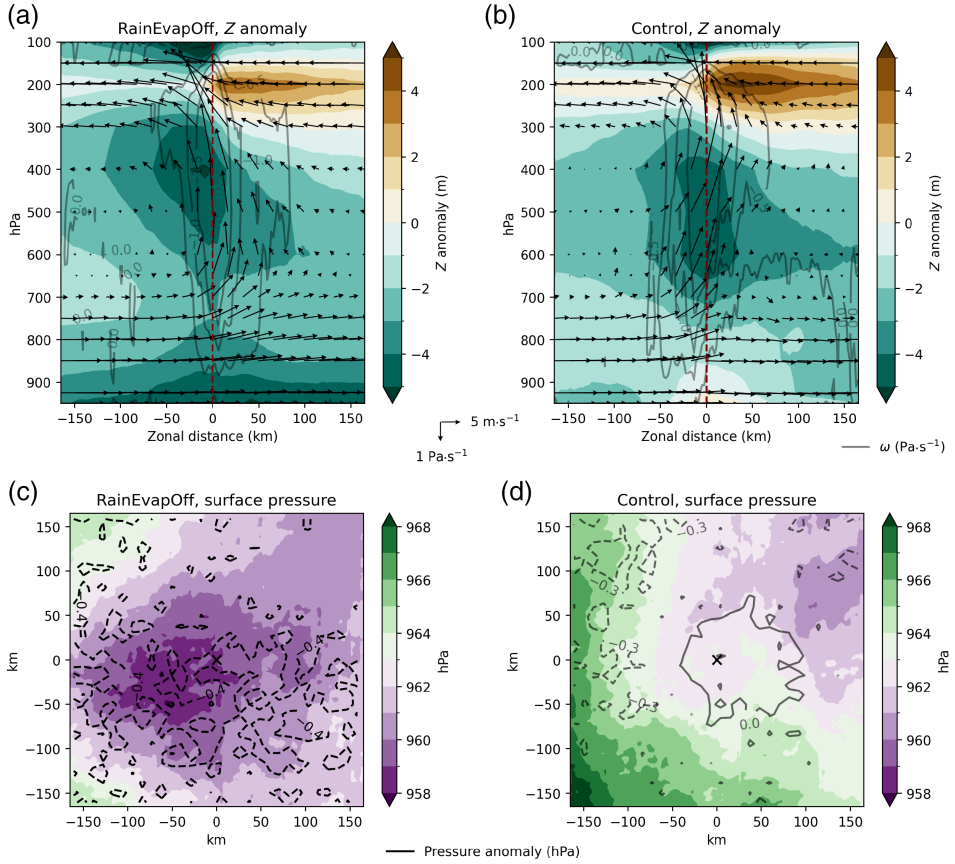

FIGURE 10 The 1800 UTC composite means of pressure field for mature mesoscale convective systems in (a, c) RainEvapOff and (b, d) Control. (a, b) Mean zonal section over 50 km central transect of geopotential height Z (shading) anomaly and vertical velocity ω in pressure coordinates (0.2 Pa · s^{-1} contours). Data plotted on pressure levels, with wind barbs as in Figure 8. (c, d) Absolute (shading) and anomalous (contours) surface pressure (hPa). In all panels, anomalies are calculated against simulation mean 1800 UTC climatology. [Colour figure can be viewed at wileyonlinelibrary.com]

strongest between 1700 and 0500 UTC, precisely the hours of peak MCS convection (Figure 5c). Both models' winds show similar diurnal cycles outside this core Sahel latitude band. Within the Sahel band, in RainEvapOff, strong convergence precedes peak convective initiation at 1500 UTC. A weakening in convergence accompanies the growth in MCSs, but overall the mean flow remains primarily convergent, with convergence strengthening from midnight. In contrast, Control shows weakened convergence preceding 1500 UTC, followed by the development of an eye of strong mean divergence at 1600 UTC that lasts through the night. This flow pattern is consistent with model and observational results from Vizy and Cook (2018).

The decrease in convergence at MCS storm-track latitudes in both experiments, simultaneous to the development of mature storms, suggests an imposition of convective downdraughts on the background flow. In RainEvapOff, where resultant cold-pool outflows are significantly suppressed, the effect is more muted and the overall mean flow remains convergent. In Control, however, where significant cold pools develop and intensify overnight (Figure 7), there is mean divergence at low levels. We find little difference in the mean convergence at 850 hPa (Supporting Information Figure S10), pointing to the key role of the strong surface density currents in Control. However, related changes in the position of the intertropical discontinuity dryline between the models will also be a significant factor (Vizy & Cook, 2018). The inhibition of cold-pool development in RainEvapOff maintains the background large-scale convergence associated with MCS initiation (Birch *et al.*, 2014a), and thus conditions suitable for maintenance of MCSs without cold pools (Crook & Moncrieff, 1988).

The mean flow in Control is, of course, far more realistic than that in the RainEvapOff sensitivity experiment. Cold-pool density currents weaken the overall monsoon flow into the Sahara, and their misrepresentation is a key source of regional model biases (Garcia-Carreras *et al.*, 2013; Marsham *et al.*, 2013). For real MCSs, whose properties and shear responses are well simulated by the Control simulation (Maybee *et al.*, 2024), our results show the key role of RKW vorticity balance in determining storm geometry. However, they also show that mature MCSs could equally be supported in this strong shear environment without any such balance (absent in Figures 8 and 10), and that RKW theory does not determine the control of shear on MCS intensities, as measured by rainfall rates, updraught velocities, and BT minima. The results in Figure 9 provide further support to the hypothesis that it is the modulation of low-level inflow by shear that is key to this control (Alfaro, 2017; Bickle *et al.*, 2022), by showing that

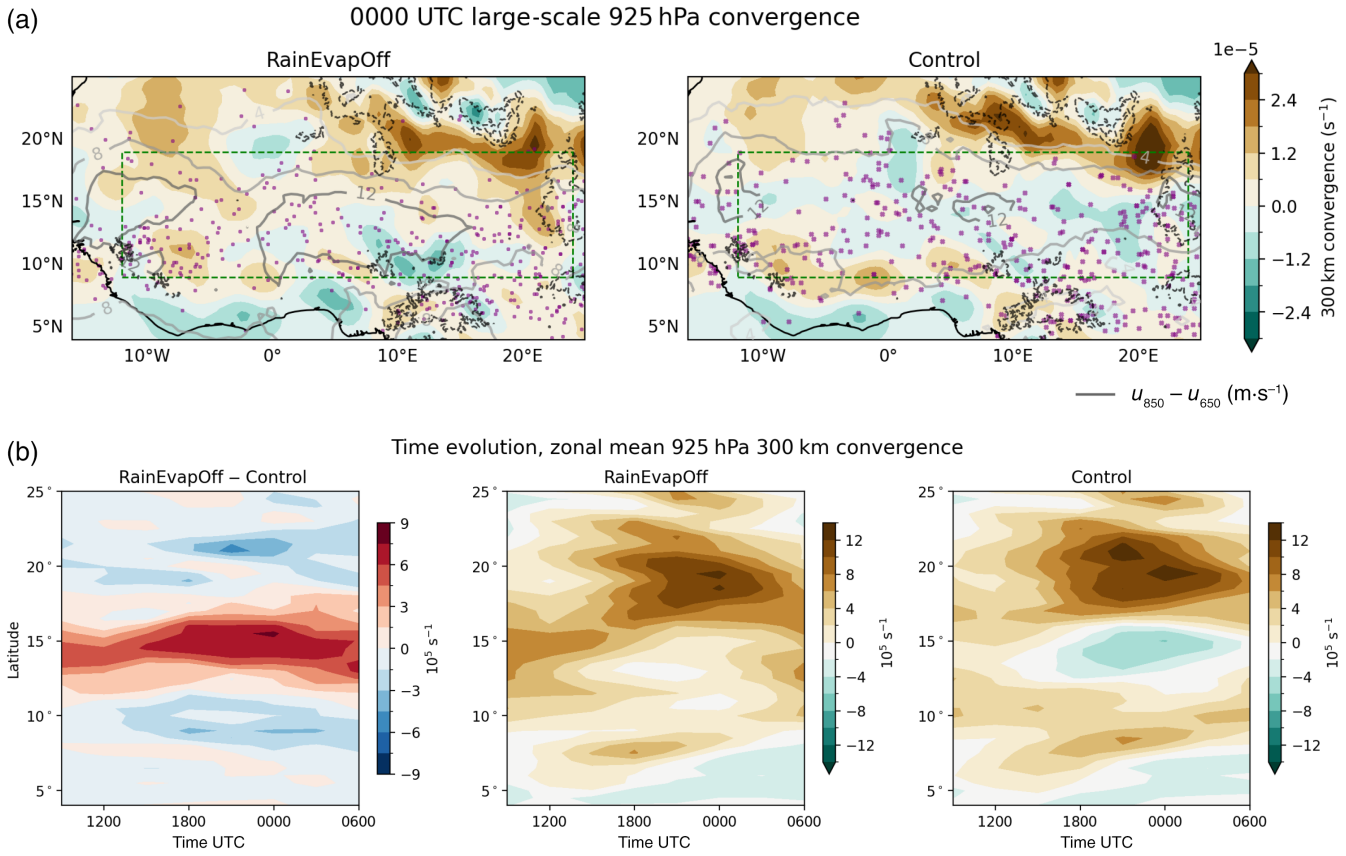

FIGURE 11 (a) Mean 300 km 0000 UTC convergence at 925 hPa in RainEvapOff and Control. Means near orography (dashed contours, 750 m and 1,500 m elevation) outside of core Sahel domain (dashed box) include winds interpolated from the surface using local lapse rate where surface pressure < 925 hPa. Solid contours and purple markers respectively plot the mean zonal shear and the mature mesoscale convective system BT_{min} locations for storms with maximum rainfall > 1 mm · hr^{-1} at 0000 UTC. (b) Hovmöller diagrams for diurnal cycle of difference and absolute values in mean zonal 925 hPa convergence, 0700 UTC to 0600 UTC. [Colour figure can be viewed at wileyonlinelibrary.com]

the (complementary) reduction of entrainment dilution in high-shear environments (Mulholland *et al.*, 2021) remains strong when cold pools are suppressed, maintaining a strong MCS shear response.

6 | CONCLUSIONS

Faced with significant uncertainties in future Sahel rainfall projections from models, our conceptual understanding of the underlying mechanisms serves an important role in guiding decision making. Cold pools play a pivotal role in the Sahel's climate through ventilation of the Sahara and transport of moisture (Trzeciak *et al.*, 2017). Disentangling their role in the observed, dynamically driven intensification of Sahel MCS rainfall (Taylor *et al.*, 2017), and contribution to MCS rainfall shear-response in CP models (Maybee *et al.*, 2024), fills key missing gaps in our knowledge of the region's mechanisms.

We have targeted the role of cold pools in Sahel MCS dynamics through a 40-day CP MetUM simulation, RainEvapOff, in which rainfall evaporation was switched off in the CASIM microphysics scheme. Compared with an unmodified Control experiment, MCSs in RainEvapOff show significantly suppressed cold pools, with an accompanying decrease in the low-level gust front, relative humidity, and temperature drop associated with the passage of an MCS. Rainfall rates are increased during the day and near the regions of most intense convective activity, but organised cold pools in Control facilitate higher nocturnal mean rainfall rates and more widespread regions of high rainfall within MCS footprints. The former result is due to an intensification in cold-pool strength overnight (Figure 7), whereas the latter likely stems from the generation of linear lines of convection along strong cold-pool boundaries in Control (Figure 2).

Using the simpleTrack storm tracking algorithm (Stein *et al.*, 2014), we find sustained nocturnal propagation of MCSs where cold pools are suppressed. Similar numbers of

very long-lived (> 10 hr) storms are found in both experiments, whereas the number of MCSs in RainEvapOff only declines significantly versus Control after 0300 UTC in the morning, but still with, on average, four storms a day persisting at 0900 UTC within the Sahel. The primary afternoon initiation of storms is unaffected by cold-pool suppression due to elevated environmental CAPE values stemming from the wetter, warmer boundary layer in RainEvapOff (Supporting Information Figure S2), and the continued presence of local convergence features independent of cold pools. There is an overall decrease in the distribution of MCS propagation speeds, which we find is explained by a decrease in the speed of the AEJ. Decreased sub-cloud cooling in RainEvapOff raises air temperatures in the Sahel, decreasing the temperature gradient with the Sahara and thus decreasing the geostrophic easterly flow. The suppression of cold-pool outflows enhances the strength of the Saharan heat low. The changes in the mean state in RainEvapOff are fully consistent with, and provide a test of, results from the Cascade project highlighting the upscale impacts of convective cold pools on African climate (Birch *et al.*, 2014b; Garcia-Carreras *et al.*, 2013; Marsham *et al.*, 2013).

Suppressing cold pools drastically changes MCS updraught geometry (Figure 8), as anticipated by RKW theory (Rotunno *et al.*, 1988), but yields no significant change in the control of environmental wind shear on MCS rainfall. Viewed together with our knowledge of storm life cycles in the two experiments, we conclude that cold pools play a pivotal role in Sahelian MCS structure—but are not fundamental to their maintenance, and do not control their environmental interactions. Tellingly, storms in both simulations show the midlevel pressure decrease across their updraughts (Figure 10) that is characteristic of mesoscale circulations (Houze, 2004; Moncrieff, 1992). Suppressing cold pools enables other dynamical mechanisms to maintain mature storms, continuing to enable the propagation of the long-lived MCSs that dominate the Sahel's climate.

In particular, our results point to the role of large-scale low-level convergence (Figure 11), and thereby gravity wave dynamics (Crook & Moncrieff, 1988). Divergent flow from cold-pool development weakens the background convergent flow that is crucial for convective initiation (Birch *et al.*, 2014a; Vizy & Cook, 2018) and propagation (Klein & Taylor, 2020) in the Sahel; eliminating rainfall evaporation suppresses this negative feedback and maintains a flow state conducive to MCS maintenance without RKW vorticity balance, as previously documented in other tropical and midlatitude domains (Grant *et al.*, 2018; Stoelinga *et al.*, 2003). In the Sahel, Tulich and Kiladis (2012) have shown fast-propagating squall lines can be better described as convectively coupled equatorial gravity waves—the detailed interactions between gravity waves and MCSs in our simulations are an important topic for future research. Meanwhile, it would be interesting to explore similar CP experiments to RainEvapOff in other MCS hotspots globally; for example, building on sensitivity experiments conducted over Taiwan (Miao & Yang, 2020).

The cold-pool sensitivity experiment presented here holds two important real-world conclusions. The first is a reinforcement of the role of the AEJ in guiding MCS propagation in the Sahel: the thermodynamic mean-state consequences of suppressing rainfall evaporation weakens the jet, causing a decrease in MCS propagation speeds. The second physical conclusion is that the intensification of MCS rainfall in stronger shear environments occurs independently of cold pools. The physics of updraught entrainment, and thus convective low-level inflow (Alfaro, 2017; Mulholland *et al.*, 2021), are the dominant mechanism. The nuanced interactions between real MCSs and vertical shear cannot be reduced solely to cold-pool dynamics.

ACKNOWLEDGEMENTS

This research was conducted through the NERC funded LMCS project (NE/W001888/1). CK also acknowledges funding from the NERC independent research fellowship COCOON (NE/X017419/1). We thank Kilian Hermes, Mitch Moncrieff, Fran Morris, Simon Peatman, Alison Stirling, and Lorenzo Tomassini for discussions that contributed to this work's progress, and Jennie Bukowski and an anonymous reviewer for thorough reviews that strengthened the manuscript. BM further thanks the Royal Meteorological Society for the award of a Rupert Ford travel grant that facilitated the development and dissemination of our results. Special thanks go to the providers of the Python packages scipy, xarray, and metpy. This work used JASMIN, the UK national collaborative data analysis facility, and the Met Office MASS data archive.

DATA AVAILABILITY STATEMENT

Access to simulation data can be provided through the JASMIN data analysis facility. The simpleTrack MCS tracking code is available at https://github.com/thmstein/simple-track, and output MCS tables and other supporting code are at https://github.com/BMaybee/MCS_shear_evaluation/tree/main/Cold_pools.

The data that support the findings of this study are available from the corresponding author upon reasonable request.

ENDNOTE

1CASIM parameters `L_prevp` and `L_arevp` enabling the evaporation of rainfall were switched to `False`.

ORCID

Ben Maybee https://orcid.org/0000-0001-7834-9489
James Bassford https://orcid.org/0009-0008-7940-3086
Paul Field https://orcid.org/0000-0001-8528-0088
Douglas J. Parker https://orcid.org/0000-0003-2335-8198

REFERENCES

Abramian, S., Muller, C. & Risi, C. (2022) Shear-convection interactions and orientation of tropical squall lines. *Geophysical Research Letters*, 49, e2021GL095184.

Abramian, S., Muller, C. & Risi, C. (2023) Extreme precipitation in tropical squall lines. *Journal of Advances in Modeling Earth Systems*, 15, e2022MS003477.

Alfaro, D.A. (2017) Low–tropospheric shear in the structure of squall lines: impacts on latent heating under layer–lifting ascent. *Journal of the Atmospheric Sciences*, 74, 229–248.

Baidu, M., Schwendike, J., Marsham, J.H. & Bain, C. (2022) Effects of vertical wind shear on intensities of mesoscale convective systems over West and Central Africa. *Atmospheric Science Letters*, 23, e1094.

Best, M.J., Pryor, M., Clark, D.B., Rooney, G.G., Essery, R., Ménard, C.B. et al. (2011) The Joint UK Land Environment Simulator (JULES), model description–Part 1: energy and water fluxes. *Geoscientific Model Development*, 4, 677–699.

Bickle, M.E., Marsham, J.H., Ross, A.N., Rowell, D.P., Parker, D.J. & Taylor, C.M. (2021) Understanding mechanisms for trends in Sahelian squall lines: roles of thermodynamics and shear. *Quarterly Journal of the Royal Meteorological Society*, 147, 983–1006.

Bickle, M.E., Marsham, J.H., Griffiths, S.D., Ross, A.N. & Crook, J. (2022) The influence of the diurnal cycle in wind shear and thermodynamics on squall lines in the West African Monsoon. *Journal of the Atmospheric Sciences*, 79, 2125–2143.

Birch, C.E., Marsham, J.H., Parker, D.J. & Taylor, C.M. (2014a) The scale dependence and structure of convergence fields preceding the initiation of deep convection. *Geophysical Research Letters*, 41, 4769–4776.

Birch, C.E., Parker, D., Marsham, J., Copsey, D. & Garcia-Carreras, L. (2014b) A seamless assessment of the role of convection in the water cycle of the West African Monsoon. *Journal of Geophysical Research: Atmospheres*, 119, 2890–2912.

Bony, S., Stevens, B., Frierson, D.M., Jakob, C., Kageyama, M., Pincus, R. et al. (2015) Clouds, circulation and climate sensitivity. *Nature Geoscience*, 8, 261–268.

Brown, A., Milton, S., Cullen, M., Golding, B., Mitchell, J. & Shelly, A. (2012) Unified modeling and prediction of weather and climate: a 25–year journey. *Bulletin of the American Meteorological Society*, 93, 1865–1877.

Bryan, G.H., Knievel, J.C. & Parker, M.D. (2006) A multimodel assessment of RKW theory's relevance to squall-line characteristics. *Monthly Weather Review*, 134, 2772–2792.

Bush, M., Boutle, I., Edwards, J., Finnenkoetter, A., Franklin, C., Hanley, K. et al. (2023) The second met office unified model–JULES regional atmosphere and land configuration, RAL2. *Geoscientific Model Development*, 16, 1713–1734.

Bush, M., Flack, D.L.A., Lewis, H.W., Bohnenstengel, S.I., Short, C.J., Franklin, C. et al. (2024) The third met office unified model–JULES regional atmosphere and land configuration, RAL3. *Geoscientific Model Development*. https://gmd.copernicus.org/preprints/gmd-2024-201/

Chen, X., Leung, L.R., Feng, Z. & Yang, Q. (2023) Environmental controls on MCS lifetime rainfall over tropical oceans. *Geophysical Research Letters*, 50, e2023GL103267.

Clark, P., Browning, K., Forbes, R., Morcrette, C., Blyth, A. & Lean, H. (2014) The evolution of an MCS over southern England. Part 2: model simulations and sensitivity to microphysics. *Quarterly Journal of the Royal Meteorological Society*, 140, 458–479.

Crook, N.A. & Moncrieff, M.W. (1988) The effect of large-scale convergence on the generation and maintenance of deep moist convection. *Journal of the Atmospheric Sciences*, 45, 3606–3624.

Crook, J., Klein, C., Folwell, S., Taylor, C.M., Parker, D.J., Stratton, R. et al. (2019) Assessment of the representation of West African storm lifecycles in convection-permitting simulations. *Earth and Space Science*, 6, 818–835.

Dione, C., Lothon, M., Badiane, D., Campistron, B., Couvreux, F., Guichard, F. et al. (2014) Phenomenology of sahelian convection observed in niamey during the early monsoon. *Quarterly Journal of the Royal Meteorological Society*, 140, 500–516.

Donahue, A.S., Caldwell, P.M., Bertagna, L., Beydoun, H., Bogenschutz, P.A., Bradley, A. et al. (2024) To exascale and beyond–The Simple Cloud-Resolving E3SM Atmosphere Model (SCREAM), a performance portable global atmosphere model for cloud-resolving scales. *Journal of Advances in Modeling Earth Systems*, 16, e2024MS004314.

Drager, A.J. & van den Heever, S.C. (2017) Characterizing convective cold pools. *Journal of Advances in Modeling Earth Systems*, 9, 1091–1115.

Engerer, N.A., Stensrud, D.J. & Coniglio, M.C. (2008) Surface characteristics of observed cold pools. *Monthly Weather Review*, 136, 4839–4849.

Feng, Z., Leung, L.R., Hardin, J., Terai, C.R., Song, F. & Caldwell, P. (2023) Mesoscale convective systems in DYAMOND global convection–permitting simulations. *Geophysical Research Letters*, 50, e2022GL102603.

Feng, Z., Prein, A.F., Kukulies, J., Fiolleau, T., Jones, W.K., Maybee, B. et al. (2025) Mesoscale Convective Systems tracking Method Intercomparison (MCSMIP): application to DYAMOND global km-scale simulations. *Journal of Geophysical Research: Atmospheres*, 130, e2024JD042204.

Field, P.R., Hill, A., Shipway, B., Furtado, K., Wilkinson, J., Miltenberger, A. et al. (2023) Implementation of a double moment cloud microphysics scheme in the UK met office regional numerical weather prediction model. *Quarterly Journal of the Royal Meteorological Society.*, 149, 703–739.

Fuglestvedt, H.F. & Haerter, J.O. (2020) Cold pools as conveyor belts of moisture. *Geophysical Research Letters*, 47, e2020GL087319.

Garcia-Carreras, L., Marsham, J., Parker, D., Bain, C., Milton, S., Saci, A. et al. (2013) The impact of convective cold pool outflows on model biases in the Sahara. *Geophysical Research Letters*, 40, 1647–1652.

Garcia-Carreras, L., Marsham, J.H., Stratton, R.A. & Tucker, S. (2021) Capturing convection essential for projections of climate change in African dust emission. *Npj Climate and Atmospheric Science*, 4, 44.

Grant, L.D., Lane, T.P. & van den Heever, S.C. (2018) The role of cold pools in tropical oceanic convective systems. *Journal of the Atmospheric Sciences*, 75, 2615–2634.

Grant, L.D., Moncrieff, M.W., Lane, T.P. & van den Heever, S.C. (2020) Shear-parallel tropical convective systems: importance of cold pools and wind shear. *Geophysical Research Letters*, 47, e2020GL087720.

Hoeller, J., Haerter, J.O. & Da Silva, N.A. (2024) Characteristics of station-derived convective cold pools over equatorial Africa. *Geophysical Research Letters*, 51, e2023GL107308.

Hohenegger, C., Korn, P., Linardakis, L., Redler, R., Schnur, R., Adamidis, P. et al. (2023) ICON–Sapphire: simulating the components of the Earth system and their interactions at kilometer and subkilometer scales. *Geoscientific Model Development*, 16, 779–811.

Houze, R.A., Jr. (2004) Mesoscale convective systems. *Reviews of Geophysics*, 42, RG4003.

Hsiao, W.-T., Maloney, E.D., Leitmann-Niimi, N.M. & Kummerow, C.D. (2024) Observed relationships between sea surface temperature, vertical wind shear, tropical organized deep convection, and radiative effects. *Journal of Climate*, 37, 1277–1293.

Jeevanjee, N. & Romps, D.M. (2013) Convective self-aggregation, cold pools, and domain size. *Geophysical Research Letters*, 40, 994–998.

Jones, R.W., Sanchez, C., Lewis, H., Warner, J., Webster, S. & Macholl, J. (2023) Impact of domain size on tropical precipitation within explicit convection simulations. *Geophysical Research Letters*, 50, e2023GL104672.

Khairoutdinov, M. & Randall, D. (2006) High-resolution simulation of shallow-to-deep convection transition over land. *Journal of the Atmospheric Sciences*, 63, 3421–3436.

Klein, C. & Taylor, C.M. (2020) Dry soils can intensify mesoscale convective systems. *Proceedings of the National Academy of Sciences*, 117, 21132–21137.

Klein, C., Jackson, L.S., Parker, D.J., Marsham, J.H., Taylor, C.M., Rowell, D.P. et al. (2021) Combining CMIP data with a regional convection-permitting model and observations to project extreme rainfall under climate change. *Environmental Research Letters*, 16, 104023.

Lane, T.P. & Zhang, F. (2011) Coupling between gravity waves and tropical convection at mesoscales. *Journal of the Atmospheric Sciences*, 68, 2582–2598.

Liu, C. & Moncrieff, M.W. (2004) Effects of convectively generated gravity waves and rotation on the organization of convection. *Journal of the Atmospheric Sciences*, 61, 2218–2227.

Mapes, B.E. (1993) Gregarious tropical convection. *Journal of the Atmospheric Sciences*, 50, 2026–2037.

Mapes, B.E., Warner, T.T. & Xu, M. (2003) Diurnal patterns of rainfall in northwestern South America. Part III: diurnal gravity waves and nocturnal convection offshore. *Monthly Weather Review*, 131, 830–844.

Marsham, J.H., Knippertz, P., Dixon, N.S., Parker, D.J. & Lister, G.M. (2011) The importance of the representation of deep convection for modeled dust-generating winds over West Africa during summer. *Geophysical Research Letters*, 38, L16803.

Marsham, J.H., Dixon, N.S., Garcia-Carreras, L., Lister, G.M., Parker, D.J., Knippertz, P. et al. (2013) The role of moist convection in the West African monsoon system: insights from continental–scale convection–permitting simulations. *Geophysical Research Letters*, 40, 1843–1849.

Mathon, V., Laurent, H. & Lebel, T. (2002) Mesoscale convective system rainfall in the sahel. *Journal of Applied Meteorology and Climatology*, 41, 1081–1092.

Maurer, V., Bischoff-Gauß, I., Kalthoff, N., Gantner, L., Roca, R. & Panitz, H.-J. (2017) Initiation of deep convection in the Sahel in a convection-permitting climate simulation for northern Africa. *Quarterly Journal of the Royal Meteorological Society*, 143, 806–816.

Maybee, B., Marsham, J., Klein, C., Parker, D.J., Barton, E.J., Taylor, C.M. et al. (2024) Wind shear effects in convection–permitting models influence mcs rainfall and forcing of tropical circulation. *Geophysical Research Letters*, 51, e2024GL110119.

Meyer, B. & Haerter, J.O. (2020) Mechanical forcing of convection by cold pools: collisions and energy scaling. *Journal of Advances in Modeling Earth Systems*, 12, e2020MS002281.

Miao, J.-E. & Yang, M.-J. (2020) A modeling study of the severe afternoon thunderstorm event at Taipei on 14 June 2015: the roles of sea breeze, microphysics, and terrain. *Journal of the Meteorological Society of Japan. Ser. II*, 98, 129–152.

Moncrieff, M.W. (1992) Organized convective systems: archetypal dynamical models, mass and momentum flux theory, and parametrization. *Quarterly Journal of the Royal Meteorological Society*, 118, 819–850.

Mulholland, J.P., Peters, J.M. & Morrison, H. (2021) How does vertical wind shear influence entrainment in squall lines? *Journal of the Atmospheric Sciences*, 78, 1931–1946.

Pandya, R.E. & Durran, D.R. (1996) The influence of convectively generated thermal forcing on the mesoscale circulation around squall lines. *Journal of the Atmospheric Sciences*, 53, 2924–2951.

Parker, D.J. & Diop-Kane, M. (2017) *Meteorology of tropical West Africa: the forecasters' handbook*. Chichester, West Sussex: John Wiley & Sons.

Prein, A.F., Liu, C., Ikeda, K., Trier, S.B., Rasmussen, R.M., Holland, G.J. et al. (2017) Increased rainfall volume from future convective storms in the US. *Nature Climate Change*, 7, 880–884.

Prein, A.F., Rasmussen, R.M., Wang, D. & Giangrande, S.E. (2021) Sensitivity of organized convective storms to model grid spacing in current and future climates. *Philosophical Transactions of the Royal Society A*, 379, 20190546.

Provod, M., Marsham, J., Parker, D. & Birch, C. (2016) A characterization of cold pools in the West African Sahel. *Monthly Weather Review*, 144, 1923–1934.

Rackow, T., Pedruzo-Bagazgoitia, X., Becker, T., Milinski, S., Sandu, I., Aguridan, R. et al. (2024) Multi-year simulations at kilometre scale with the integrated forecasting system coupled to FESOM2. *5/NEMOv3. 4. EGUsphere*, 2024, 1–59.

Robe, F.R. & Emanuel, K.A. (2001) The effect of vertical wind shear on radiative–convective equilibrium states. *Journal of the Atmospheric Sciences*, 58, 1427–1445.

Rotunno, R., Klemp, J.B. & Weisman, M.L. (1988) A theory for strong, long-lived squall lines. *Journal of Atmospheric Sciences*, 45, 463–485.

Schumacher, R.S. (2009) Mechanisms for quasi-stationary behavior in simulated heavy-rain-producing convective systems. *Journal of the Atmospheric Sciences*, 66, 1543–1568.

Senior, C.A., Marsham, J.H., Berthou, S., Burgin, L.E., Folwell, S.S., Kendon, E.J. et al. (2021) Convection permitting regional climate change simulations for understanding future climate and informing decision making in Africa. *Bulletin of the American Meteorological Society*, 102, 1–46.

Slingo, J., Bates, P., Bauer, P., Belcher, S., Palmer, T., Stephens, G. et al. (2022) Ambitious partnership needed for reliable climate prediction. *Nature Climate Change*, 12, 499–503.

Stein, T.H., Hogan, R.J., Hanley, K.E., Nicol, J.C., Lean, H.W., Plant, R.S. et al. (2014) The three-dimensional morphology of simulated and observed convective storms over southern England. *Monthly Weather Review*, 142, 3264–3283.

Stoelinga, M.T., Locatelli, J.D., Schwartz, R.D. & Hobbs, P.V. (2003) Is a cold pool necessary for the maintenance of a squall line produced by a cold front aloft? *Monthly Weather Review*, 131, 95–115.

Taylor, C.M., Gounou, A., Guichard, F., Harris, P.P., Ellis, R.J., Couvreux, F. et al. (2011) Frequency of Sahelian storm initiation enhanced over mesoscale soil-moisture patterns. *Nature Geoscience*, 4, 430–433.

Taylor, C.M., Belušić, D., Guichard, F., Parker, D.J., Vischel, T., Bock, O. et al. (2017) Frequency of extreme Sahelian storms tripled since 1982 in satellite observations. *Nature*, 544, 475–478.

Thorpe, A., Miller, M. & Moncrieff, M. (1982) Two–dimensional convection in non–constant shear: a model of mid–latitude squall lines. *Quarterly Journal of the Royal Meteorological Society*, 108, 739–762.

Tomassini, L., Willett, M., Sellar, A., Lock, A., Walters, D., Whitall, M. et al. (2023) Confronting the convective gray zone in the global configuration of the Met Office Unified Model. *Journal of Advances in Modeling Earth Systems*, 15, e2022MS003418.

Tompkins, A.M. (2001) Organization of tropical convection in low vertical wind shears: the role of cold pools. *Journal of the Atmospheric Sciences*, 58, 1650–1672.

Torri, G., Kuang, Z. & Tian, Y. (2015) Mechanisms for convection triggering by cold pools. *Geophysical Research Letters*, 42, 1943–1950.

Trier, S.B., Marsham, J.H., Davis, C.A. & Ahijevych, D.A. (2011) Numerical simulations of the postsunrise reorganization of a nocturnal mesoscale convective system during 13 June IHOP_2002. *Journal of the Atmospheric Sciences*, 68, 2988–3011.

Trzeciak, T.M., Garcia-Carreras, L. & Marsham, J.H. (2017) Cross-Saharan transport of water vapor via recycled cold pool outflows from moist convection. *Geophysical Research Letters*, 44, 1554–1563.

Tulich, S.N. & Kiladis, G.N. (2012) Squall lines and convectively coupled gravity waves in the tropics: why do most cloud systems propagate westward? *Journal of the Atmospheric Sciences*, 69, 2995–3012.

Tulich, S.N. & Mapes, B.E. (2008) Multiscale convective wave disturbances in the tropics: insights from a two-dimensional cloud-resolving model. *Journal of the Atmospheric Sciences*, 65, 140–155.

Van Weverberg, K., Morcrette, C.J., Boutle, I., Furtado, K. & Field, P.R. (2021) A bimodal diagnostic cloud fraction parameterization. Part I: motivating analysis and scheme description. *Monthly Weather Review*, 149, 841–857.

Vizy, E.K. & Cook, K.H. (2018) Mesoscale convective systems and nocturnal rainfall over the West African Sahel: role of the Inter-tropical front. *Climate Dynamics*, 50, 587–614.

Weisman, M.L. & Rotunno, R. (2004) A theory for strong long-lived squall lines revisited. *Journal of the Atmospheric Sciences*, 61, 361–382.

Yang, M.-J. & Houze, R.A. (1996) Momentum budget of a squall line with trailing stratiform precipitation: calculations with a high-resolution numerical model. *Journal of the Atmospheric Sciences*, 53, 3629–3652.

Yang, G.-Y. & Slingo, J. (2001) The diurnal cycle in the tropics. *Monthly Weather Review*, 129, 784–801.

Zhao, S., Cook, K.H. & Vizy, E.K. (2024) Greenhouse gas-induced modification of intense storms over the west african sahel through thermodynamic and dynamic processes. *Climate Dynamics*, 62, 1–26.

SUPPORTING INFORMATION

Additional supporting information can be found online in the Supporting Information section at the end of this article.

How to cite this article: Maybee, B., Bassford, J., Marsham, J.H., Lewis, H., Field, P., Klein, C. *et al.* (2025) How sensitive are Sahelian mesoscale convective systems to cold-pool suppression?. *Quarterly Journal of the Royal Meteorological Society*, e5032. Available from: https://doi.org/10.1002/qj.5032